

Six New Compact Triply Eclipsing Triples Found With *TESS*

S. A Rappaport^{1*}, T. Borkovits^{2,3,4,5}, R. Gagliano⁶, T. L. Jacobs⁷, V. B. Kostov^{8,9},
 B. P. Powell⁸, I. Terentev¹⁰, M. Omohundro¹⁰, G. Torres¹¹, A. Vanderburg¹,
 T. Mitnyan^{2,12}, M. H. Kristiansen^{13,14}, D. LaCourse¹⁵, H. M. Schwengeler¹⁰,
 T. G. Kaye¹⁶, A. Pál^{3,17}, T. Pribulla¹⁸, I. B. Bíró², I. Csányi², Z. Garai^{4,5,18},
 P. Zasche¹⁹, P. F. L. Maxted²⁰, J. E. Rodriguez²¹, D. J. Stevens^{22,23}

¹ Department of Physics, Kavli Institute for Astrophysics and Space Research, M.I.T., Cambridge, MA 02139, USA

² Baja Astronomical Observatory of University of Szeged, H-6500 Baja, Szegedi út, Kt. 766, Hungary

³ Konkoly Observatory, Research Centre for Astronomy and Earth Sciences, H-1121 Budapest, Konkoly Thege Miklós út 15-17, Hungary

⁴ ELTE Eötvös Loránd University, Gothard Astrophysical Observatory, Szent Imre h. u. 112, 9700 Szombathely, Hungary

⁵ MTA-ELTE Exoplanet Research Group, H-9700 Szombathely, Szent Imre h. u. 112, Hungary

⁶ Amateur Astronomer, Glendale, AZ 85308

⁷ Amateur Astronomer, 12812 SE 69th Place Bellevue, WA 98006, USA

⁸ NASA Goddard Space Flight Center, 8800 Greenbelt Road, Greenbelt, MD 20771, USA

⁹ SETI Institute, 189 Bernardo Avenue, Suite 200, Mountain View, CA 94043, USA

¹⁰ Citizen Scientist, c/o Zooniverse, Dept. of Physics, University of Oxford, Denys Wilkinson Building, Keble Road, Oxford, OX1 3RH, UK

¹¹ Center for Astrophysics | Harvard & Smithsonian, 60 Garden St., Cambridge, MA 02138, USA

¹² Department of Experimental Physics, University of Szeged, 6720 Szeged, Dóm tér 9, Hungary

¹³ Brorfelde Observatory, Observator Gyldenkernes Vej 7, DK-4340 Tølløse, Denmark

¹⁴ National Space Institute, Technical University of Denmark, Elektrovej 327, DK-2800 Lyngby, Denmark

¹⁵ Amateur Astronomer, 7507 52nd Place NE Marysville, WA 98270, USA

¹⁶ Foundation for Scientific Advancement, Patterson Observatory, AZ

¹⁷ Kavli Institute for Astrophysics and Space Research, M.I.T., Cambridge, MA 02139, USA

¹⁸ Astronomical Institute, Slovak Academy of Sciences, 05960 Tatranská Lomnica, Slovakia

¹⁹ Astronomical Institute, Charles University, Faculty of Mathematics and Physics, V Holešovičkách 2, CZ-180 00, Praha 8, Czech Republic

²⁰ Astrophysics Group, Keele University, Staffordshire, ST5 5BG, UK

²¹ Department of Physics and Astronomy, Michigan State University, East Lansing, MI 48824, USA

²² Department of Astronomy & Astrophysics, The Pennsylvania State University, 525 Davey Lab, University Park, PA 16802, USA

²³ Center for Exoplanets and Habitable Worlds, The Pennsylvania State University, 525 Davey Lab, University Park, PA 16802, USA

Accepted XXX. Received YYY; in original form ZZZ

ABSTRACT

In this work we report the discovery and analysis of six new compact triply eclipsing triple star systems found with the *TESS* mission: TICs 37743815, 42565581, 54060695, 178010808, 242132789, and 456194776. All of these exhibit distinct third body eclipses where the inner eclipsing binary (EB) occults the third ('tertiary') star, or vice versa. We utilized the *TESS* photometry, archival photometric data, and available archival spectral energy distribution curves (SED) to solve for the properties of all three stars, as well as many of the orbital elements. We describe in detail our SED fits, search of the archival data for the outer orbital period, and the final global photodynamical analyses. From these analyses we find that all six systems are coplanar to within $0^\circ - 5^\circ$, and are viewed nearly edge on (i.e., within a couple of degrees). The outer orbital periods and eccentricities of the six systems are $\{P_{\text{out}} \text{ (days)}, e\}$: $\{68.7, 0.36\}$, $\{123, 0.16\}$, $\{60.7, 0.01\}$, $\{69.0, 0.29\}$, $\{41.5, 0.01\}$, $\{93.9, 0.29\}$, respectively, in the order the sources are listed above. The masses of all 12 EB stars were in the range of $0.7\text{--}1.8 M_\odot$ and were situated near the main sequence. By contrast, the masses and radii of the tertiary stars ranged from $1.5\text{--}2.3 M_\odot$ and $2.9\text{--}12 R_\odot$, respectively. We use this information to estimate the occurrence rate of compact flat triple systems.

Key words: binaries:eclipsing – binaries:close – stars:individual: TIC 37743815 – stars:individual: TIC 42565581 – stars:individual: TIC 54060695 – stars:individual: TIC 178010808 – stars:individual: TIC 242132789 – stars:individual: TIC 456194776

1 INTRODUCTION

* E-mail: sar@mit.edu

al. 2010), *K2* (Howell et al. 2014), and *TESS* (Ricker et al. 2015), it has become relatively easy to discover triply eclipsing triple star systems. These are often found when an extra, isolated pair of eclipses appear in the lightcurve of an ordinary eclipsing binary (EB), or a long exotic-looking extra eclipse appears that cannot be produced in a simple binary (see the recent extensive review of Borkovits 2022). We refer to these as ‘third-body’ events where either the EB occults the third star (hereafter, the ‘tertiary’) in its outer orbit, or vice versa. Typical eclipse periods for the inner EBs are days, while the period for the extra third-body eclipses range from a month to about a year. When one of these triples is found, no further vetting of the object is typically needed before concluding that this is a bound triple system (or possibly a higher stellar multiple). By contrast, when a pair of EBs is found in the same photometric aperture, it is not immediately clear whether the two EBs are physically bound or are simply close together in the sky by chance (see the quadruples catalog of Kostov et al. 2022), and further vetting in the form of, e.g., radial velocity measurements (RVs) or eclipse timing variations (ETVs) is required.

Once a compact triple system has been identified via its third body eclipses, several additional characteristics can quickly become apparent about the system. First, if more than one outer eclipse of the same type¹ are seen in succession, then the outer orbital period of the triple is immediately revealed. If both the primary and secondary outer eclipses are seen, then, just as in an ordinary EB, the quantity $e_{\text{out}} \cos \omega_{\text{out}}$ can be measured, where e_{out} and ω_{out} are the eccentricity and argument of periastron of the outer orbit, respectively. Finally, the presence of both inner and outer eclipses gives some good indication that the binary orbital plane and the outer orbital plane are at least somewhat aligned (i.e., the systems tend to be ‘flat’) or else the likelihood of detecting both sets of eclipses is relatively lower.

As we and others have shown in a number of previous papers (see, e.g. Carter et al. 2011; Borkovits et al. 2013; Madsuda et al. 2015; Orosz 2015; Alonso et al. 2015; Borkovits et al. 2019a, 2020b, 2022), the outer eclipses have encoded in them a substantial amount of information which, when combined with supplementary data, can ultimately lead to a complete description of the stellar properties (masses, radii, T_{eff} , age, and metallicity) as well as the complete orbital configuration of the system. The supplemental material can involve the EB lightcurve itself, the extracted ETV curve, spectral energy distribution (SED) measurements from archival surveys, ground-based photometric surveys, and RVs.

Another feature of compact triple star systems that makes them fascinating objects to study is the relatively short timescales for dynamical interactions. These can occur over a year, a few months, or even weeks. Interesting effects to look for include dynamical as well as light-travel time delays in the ETVs of the EBs, forced apsidal motion in the EB, orbital plane precession if the two orbital planes are misaligned, and even large amplitude von Zeipel-Kozai-Lidov cycles (von Zeipel 1910; Lidov 1962; Kozai 1962) in the case of strongly misaligned orbital planes.

Triple star systems are also interesting in terms of the

insight they provide about the formation and subsequent evolution of multistellar systems (see, e.g., Tokovinin 2021; Borkovits 2022; Sect. 7). They are the next simplest entity after binary star systems. In some ways they are analogous to studying He atoms after mastering H atoms. However, while there are more than a million eclipsing binary systems known (see, e.g., Sect. 2; Powell et al. 2021; E. Kruse, 2022 in preparation), the number of triply eclipsing triple systems in the literature, is currently under 20.

Here we present the discovery and detailed analyses of six new compact triply eclipsing triple star systems. In Section 2 we discuss how the discovery of the third body events were made using the *TESS* data, and present plots of the third body events. Archival spectral energy distributions (SED) are then used in Section 3 to make first estimates of the constituent stellar masses, radii, and T_{eff} . We then use archival photometric data from a number of ground-based surveys to determine the outer orbital period of the triples via the third-body eclipses (see Sect. 4). The detailed photodynamical model by which we analyze jointly the photometric lightcurves, eclipse timing variations, and spectral energy distributions is reviewed in Section 5. The system parameters for each of the six triple systems are presented in Section 6 in the form of comprehensive tables, including extracted masses, radii, and effective temperatures, as well as the orbital parameters for both the inner and outer orbits. We summarize our results and discuss a few of the salient findings from our study in Section 7. We also discuss how our compact triple systems may inform us about multistellar formation and evolution.

2 DISCOVERY OF TRIPLY ECLIPSING TRIPLES WITH *TESS*

Our ‘Visual Survey Group’ (VSG; Kristiansen et al. 2022) continues to search for multi-stellar systems in the *TESS* lightcurves. We estimate that, thus far, we have visually inspected some 10 million lightcurves from *TESS*. Such visual searches are a complement to more automated ones using machine learning algorithms (see, e.g., Powell et al. 2021; Kostov et al. 2021; Kostov et al. 2022). The lightcurves are displayed with Allan Schmitt’s `LcTools` and `LcViewer` software (Schmitt et al. 2019), which allows for an inspection of a typical lightcurve in just \sim 5 seconds. It is important to note that 9 million of the studied lightcurves were of anonymous stars, while 1 million lightcurves were of preselected eclipsing binaries that were found in the *TESS* data via machine learning searches (see Powell et al. 2021; E. Kruse, 2022 in preparation).

For our survey work we largely made use of lightcurves from the following sources: Science Processing Operations Center (SPOC, Jenkins et al. 2016); the Difference Imaging Pipeline (Oelkers & Stassun 2018); the PSF-based Approach to TESS High quality data Of Stellar clusters (PATHOS, Nardiello et al. 2019); the Cluster Difference Imaging Photometric Survey (CDIPS, Bouma et al. 2019); the MIT Quick Look Pipeline (QLP, Huang et al. 2020); the TESS Image CALibrator Full Frame Images (TICA, Fausnaugh et al. 2020); and the Goddard Space Flight Center (GSFC, see Sect. 2, Powell et al. 2021).

The first signatures that are looked for in terms of identifying triply eclipsing triples are an eclipsing binary lightcurve

¹ As in ordinary EBs, outer eclipses come in two flavors—primary and secondary eclipses.

Table 1. Main properties of the six triple systems from different catalogs

Parameter	TIC 37743815	TIC 42565581	TIC 54060695	TIC 178010808	TIC 242132789	TIC 456194776
RA (J2000)	06 : 15 : 28.89	06 : 26 : 37.58	06 : 56 : 14.83	07 : 33 : 05.27	06 : 14 : 26.95	03 : 28 : 29.41
Dec (J2000)	-29 : 39 : 12.14	-03 : 23 : 50.66	-25 : 25 : 14.49	-04 : 23 : 20.36	-04 : 08 : 12.48	43 : 36 : 44.56
T^a	12.928 ± 0.007	12.867 ± 0.014	12.132 ± 0.022	12.132 ± 0.007	12.636 ± 0.009	11.766 ± 0.008
G^b	13.479 ± 0.001	13.433 ± 0.001	12.679 ± 0.001	12.531 ± 0.000	13.492 ± 0.001	12.243 ± 0.001
G_{BP}^b	13.939 ± 0.003	13.955 ± 0.005	13.123 ± 0.003	12.837 ± 0.001	14.325 ± 0.004	12.620 ± 0.002
G_{RP}^b	12.859 ± 0.002	12.748 ± 0.002	12.060 ± 0.002	12.062 ± 0.001	12.582 ± 0.003	11.690 ± 0.001
B^a	14.639 ± 0.035	14.626 ± 0.044	13.755 ± 0.112	13.320 ± 0.071	15.454 ± 0.073	12.801 ± 0.396
V^c	13.767 ± 0.126	14.010 ± 0.183	12.884 ± 0.080	12.649 ± 0.069	13.869 ± 0.103	11.997 ± 0.029
J^d	12.075 ± 0.023	11.794 ± 0.023	11.254 ± 0.023	11.544 ± 0.024	11.211 ± 0.021	11.069 ± 0.025
H^d	11.664 ± 0.027	11.335 ± 0.025	10.836 ± 0.023	11.305 ± 0.025	10.560 ± 0.023	10.777 ± 0.029
K^d	11.527 ± 0.021	11.158 ± 0.021	10.735 ± 0.023	11.224 ± 0.025	10.347 ± 0.022	10.705 ± 0.022
$W1^e$	11.476 ± 0.023	11.102 ± 0.023	10.661 ± 0.023	11.221 ± 0.023	10.223 ± 0.022	10.644 ± 0.023
$W2^e$	11.497 ± 0.021	11.149 ± 0.020	10.706 ± 0.020	11.241 ± 0.021	10.259 ± 0.020	10.647 ± 0.021
$W3^e$	11.463 ± 0.149	11.266 ± 0.131	10.597 ± 0.087	11.247 ± 0.140	10.270 ± 0.089	10.617 ± 0.099
$T_{\text{eff}} \text{ (K)}^b$	5039 ± 100	4895 ± 175	5029 ± 220	5862 ± 30	4015 ± 135	5375 ± 550
$T_{\text{eff}} \text{ (K)}^a$	5135 ± 125	5374 ± 135	5660 ± 125	6090 ± 126	4593 ± 123	6690 ± 62
$R \text{ (R}_{\odot})^b$	4.73 ± 0.18	8.43 ± 0.60	8.96 ± 0.68	4.12 ± 0.04	14.5 ± 0.9	7.06 ± 1.30
$R \text{ (R}_{\odot})^a$	4.46 ± <i>NA</i>	7.97 ± <i>NA</i>	7.79 ± <i>NA</i>	3.85 ± 0.28	13.3 ± <i>NA</i>	5.14 ± <i>NA</i>
Distance (pc) ^f	1857 ± 39	3281 ± 160	2221 ± 50	1464 ± 30	3258 ± 165	1590 ± 40
$E(B - V)^a$	0.036 ± 0.006	0.213 ± 0.017	0.168 ± 0.033	0.046 ± 0.006	0.336 ± 0.011	0.167 ± <i>NA</i>
$\mu_{\alpha} \text{ (mas yr}^{-1}\text{)}^b$	-0.13 ± 0.01	+0.81 ± 0.02	-2.32 ± 0.01	-2.03 ± 0.01	0.63 ± 0.02	-0.18 ± 0.02
$\mu_{\delta} \text{ (mas yr}^{-1}\text{)}^b$	+7.58 ± 0.01	-1.03 ± 0.02	+3.26 ± 0.01	-1.17 ± 0.01	-1.31 ± 0.02	-2.74 ± 0.01

Notes. (a) TESS Input Catalog (TIC v8.2) (Paegert et al. 2021). (b) Gaia EDR3 (Gaia collaboration 2021); the uncertainty in T_{eff} and R listed here is 1.5 times the geometric mean of the upper and lower error bars cited in DR2. (c) AAVSO Photometric All Sky Survey (APASS) DR9, (Henden et al. 2015), <http://vizier.u-strasbg.fr/viz-bin/VizieR?-source=II/336/apass9>. (d) 2MASS catalog (Skrutskie et al. 2006). (e) WISE point source catalog (Cutri et al. 2013). (f) Bailer-Jones et al. (2021). (g) <http://argonaut.skymaps.info/query>

Table 2. TESS Observation Sectors for the Triples

Object	Sectors Observed	Third Body Events
TIC 37743815	S6 & S33	S6 & S33
TIC 42565581	S6 & S33	S6 & S33
TIC 54060695	S6 & S7 & S33	S6 & S7 & S33
TIC 178010808	S7 & S34	S7
TIC 242132789	S6 & S33	S6 & S33
TIC 456194776	S18	S18

with an additional strangely shaped extra eclipse or rapid succession of isolated eclipses. One gratifying aspect of finding triply eclipsing triples is that they are in a sense ‘self-vetted’. In particular, there is no way for a single binary, or sets of independent stars or binaries to produce such ‘extra’ eclipsing events. Therefore, additional vetting becomes largely unnecessary in proving that these are indeed triples (or possibly higher order multiples).

While searching through the lightcurves obtained from the first three full years of TESS observations we have found more than ∼50 of these triply eclipsing triples. Of these we have determined the outer orbital period for 20 of them. We have previously reported on four of these systems (Borkovits et al. 2020b; Borkovits et al. 2022). Here we present the discovery and analysis of six new triply eclipsing triples from among this set: TIC 37743815, TIC 42565581, TIC 54060695, TIC 178010808, TIC 242132789, and TIC 456194776. (See Table 1 for the main catalog data of the targets.)

All six targets were measured in full frame images from TESS with either 30-min or 10-min cadence. A portion of the TESS lightcurves for all six sources are shown in Fig.1. The sectors during which these sources were observed with TESS are summarized in Table 2. TICs 37743815, 42565581, 178010808, and 242132789 were observed during two widely separated sectors each, and a third body event was observed for each source in both sectors, except for TIC 178010808, for which only one third-body event was detected. TIC 456194776 was observed in only one sector. Finally, TIC 54060695 was observed during three sectors, with a third body event detected in each—two secondary and one primary outer eclipses.

Given that the sectors are only approximately a month long and the outer orbital periods range from 42 to 123 days, it is somewhat fortuitous that we managed to observe third body events in nearly all the sectors. However, most of these systems exhibit two eclipses per outer orbit, and we have selected these for presentation in this work precisely because the outer periods are relatively short and therefore easy to detect even in archival data sets. In other words, there are several selection effects at work here.

3 PRELIMINARY SED ANALYSIS

Once we have discovered a triply eclipsing triple, we would like to develop some initial estimates of the nature of the three stars in the system. To do this we make use of an analysis of the spectral energy distribution (SED). We utilize the VizieR (Ochsenbein et al. 2000; A.-C. Simon & T. Boch: <http://vizier.u-strasbg.fr/viz-bin/VizieR?-source=II/336/apass9>)

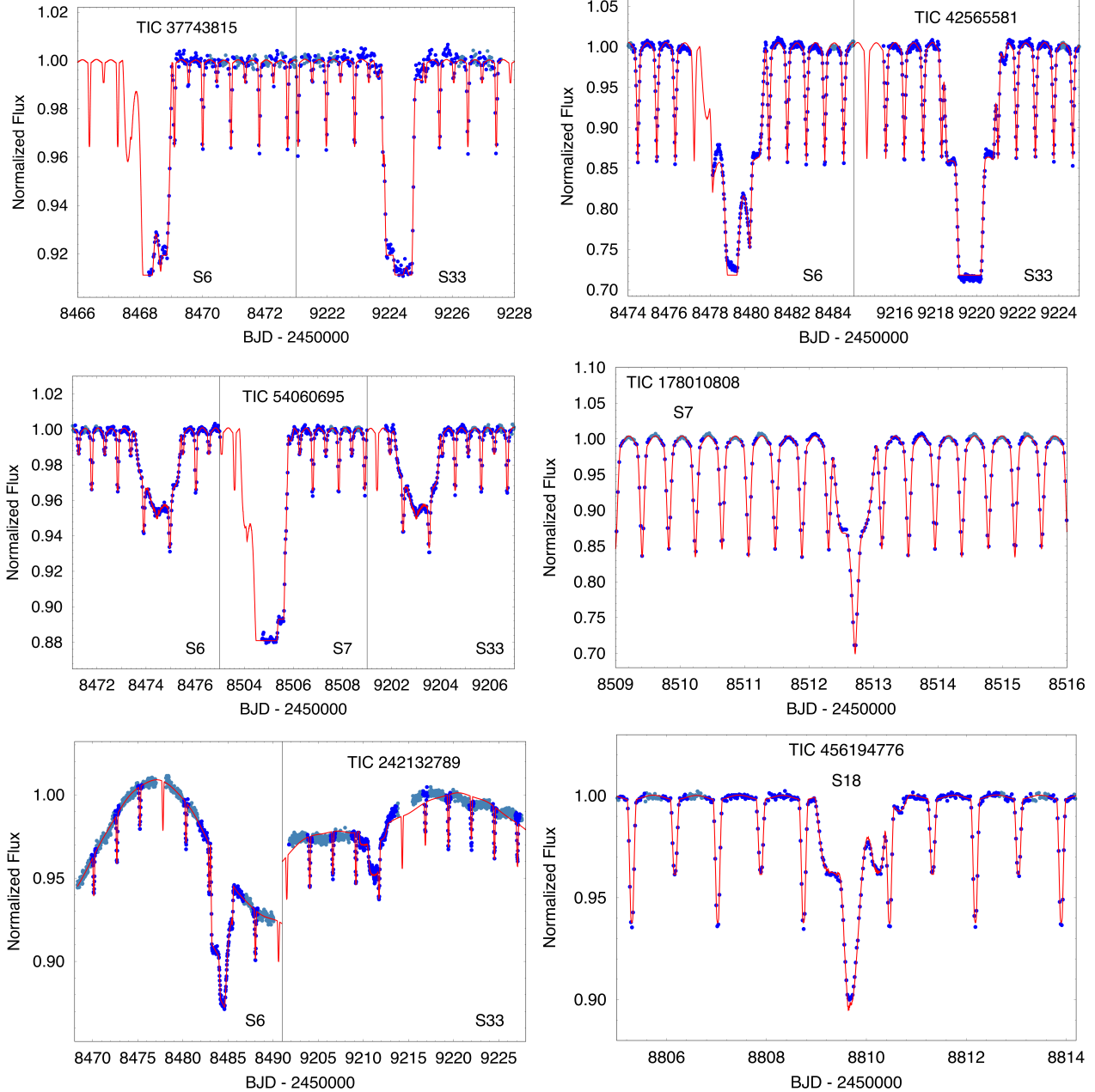


Figure 1. *TESS* third body lightcurves. We present a portion of a sector’s lightcurve for each source containing the third body event that led to their discoveries. For two of the sources there is only a single third body event that was detected, while in the other four cases we show portions of two or three orbits which exhibited third body events. The overplotted model lightcurves are discussed in Sect. 5. The lighter blue points in the out-of-eclipse region were omitted from the photodynamical fits to save computation time.

//vizier.unistra.fr/vizier/sed/) SED service which, in turn, utilizes systematic sky coverage of such surveys as Skymapper (Wolf et al. 2018), Pan-STARRS (Chambers et al. 2016), SDSS (Gunn et al. 1998), 2MASS (Skrutskie et al. 2006), WISE (Cutri et al. 2013), and in some cases Galex (Bianchi et al. 2017). These typically provide ~ 20 fluxes over the range 0.35 to 21 microns.

Unless we have specific information to the contrary, we assume for our preliminary analysis that the three stars in the system have evolved in a coeval fashion since their birth as a triple system. We further assume that there has been no

mass transfer among the three stars, in particular between the binary components. Under these assumptions, there are only four parameters that need to be fitted via a Markov chain Monte Carlo approach (see, e.g., Ford 2005; Rappaport et al. 2021): M_{Aa} , M_{Ab} , M_B , and the age of the system, where Aa and Ab refer to the stars in the inner binary, while B is the tertiary star in the outer orbit. We also make use of *MIST* stellar evolution tracks (Paxton et al. 2011; Paxton et al. 2015; Paxton et al. 2019; Dotter 2016; Choi et al.

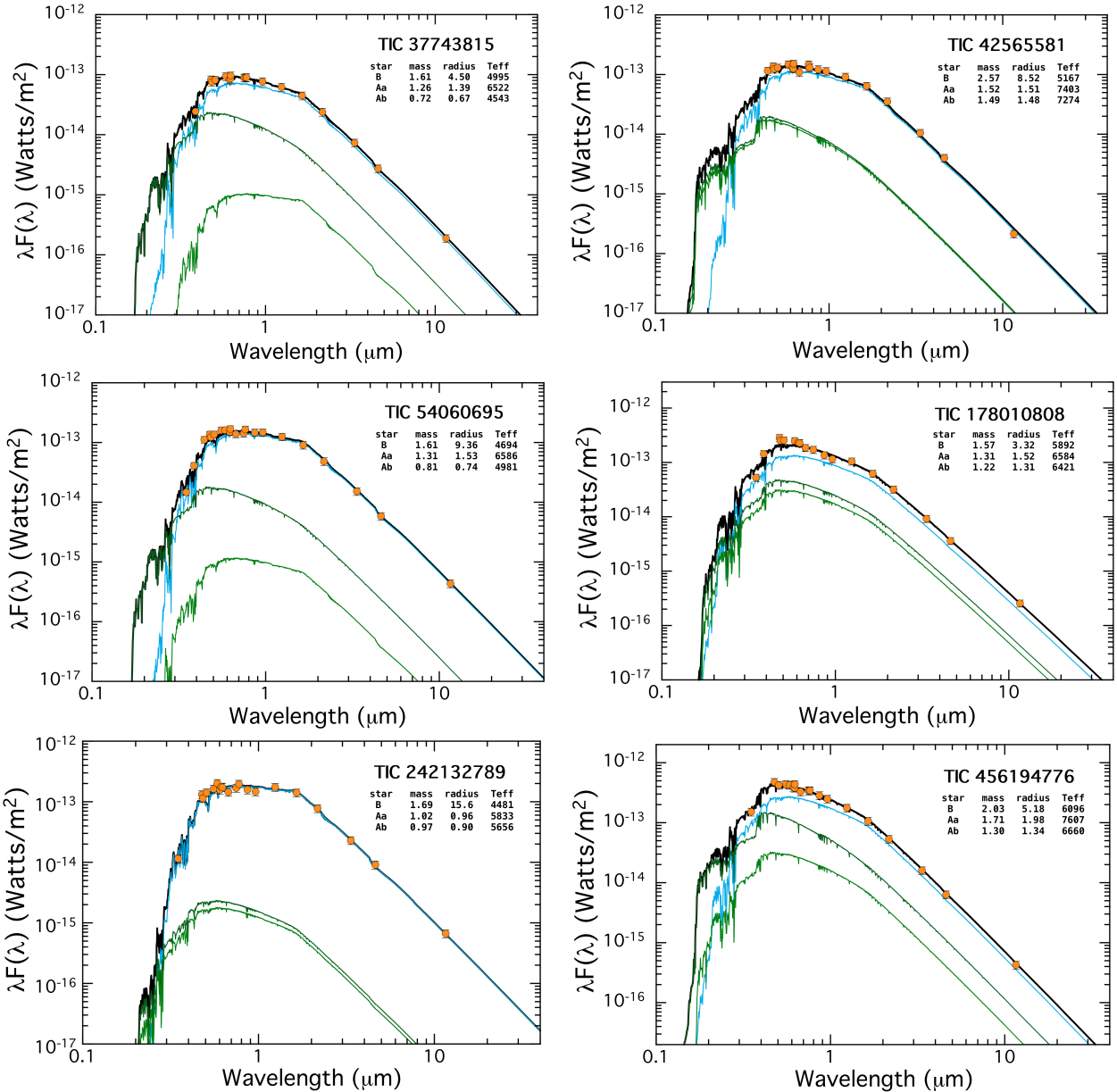


Figure 2. SED fits for each of the six triply eclipsing triples discussed in this work. The cyan curve represents the model spectrum of the tertiary star (B) while the green curves represent the EB stars (Aa and Ab). The black curve is the sum of the three model spectra. The fits for the three stellar masses, radii, and T_{eff} 's were made using only the ~ 20 measured SED points, a very loose constraint on the radius and T_{eff} for the tertiary star, and a temperature ratio for the inner EB based on eclipse depths (see Sect. 3 for details). We also explicitly make the assumption that the three stars are evolving in a coeval fashion without mass transfer. The units on the inset tables are M_{\odot} , R_{\odot} , and K. Typical formal uncertainties on the masses are $\sim 10\%$.

2016) for an assumed solar composition², as well as stellar atmosphere models from (Castelli & Kurucz 2003). If these four parameters can be determined, then the evolution tracks simultaneously determine the stellar radii and effective temperature of all three stars.

In order to fit an SED, one typically requires an accurate distance to the source and the corresponding interstellar extinction, A_V . Since Gaia (Gaia collaboration 2021) provides

² Adopted for this preliminary analysis only. See Sect. 5 for a description of the full, and more general, photodynamical analysis.

a secure distance with typically better than 5% accuracy, and we can find information on the extinction from a variety of sources (e.g., Bayestar19; Green et al. 2019), in principle we do not need to fit for these parameters. However, we usually add these two quantities to the fitted MCMC parameters, but with priors limited to just ± 4 times the listed uncertainties on them.

In spite of having some 20 SED data points to work with, and only 4-6 free parameters to fit for, this is most often quite insufficient for a decent solution. The reasons are that (i) many of the SED points are sufficiently close to each other

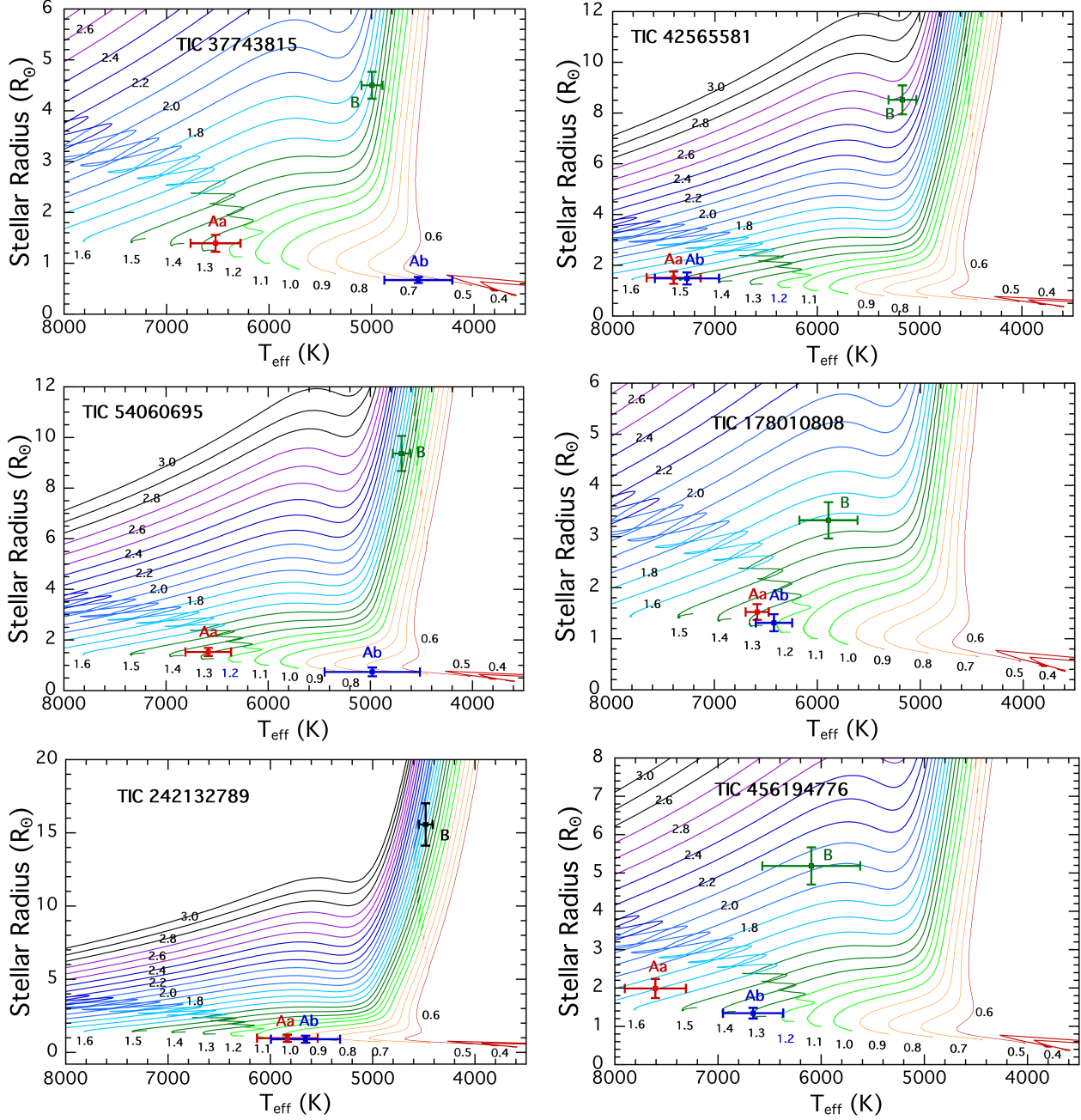


Figure 3. The locations of the three stars in each of the six triple systems shown superposed on the MIST stellar evolution tracks for stars of solar composition. The numbers next to the tracks are the stellar masses in M_{\odot} . The locations of the stars in this diagram were taken from the SED fits shown in Fig. 2. Somewhat more accurate stellar parameters are tabulated in Sect. 5 based on the full photodynamical analyses. However, the locations do not move appreciably (see Sect. 6.1).

in wavelength so that they are not really independent, and (ii) a typical SED curve contains essentially only 4 or 5 defining characteristics, e.g., flux at any given wavelength on the Rayleigh-Jeans tail, wavelength of the peak in the SED curve, sharpness of the falloff at short wavelengths, etc. Therefore, we find it extremely helpful to add a few supplementary constraints in the MCMC fit. These include estimates of the radius and T_{eff} of the tertiary and the ratio $T_{\text{eff},\text{Aa}}/T_{\text{eff},\text{Ab}}$.

Because all of the tertiary stars in this work are giants³, they tend to dominate the light from the system. Therefore, we make use of the Gaia DR2 and *TESS* Input Catalog (TIC v8.2) estimates of the ‘composite’ radius and T_{eff} of the entire system measured as a single object (see Table 1). However, because those estimates are hardly a perfect representation

³ The least evolved tertiary is the one in TIC 178010808, a 1.6 M_{\odot} star of radius $2.9 R_{\odot}$ whose luminosity exceeds that of the combined EB stars by nearly a factor of 2.

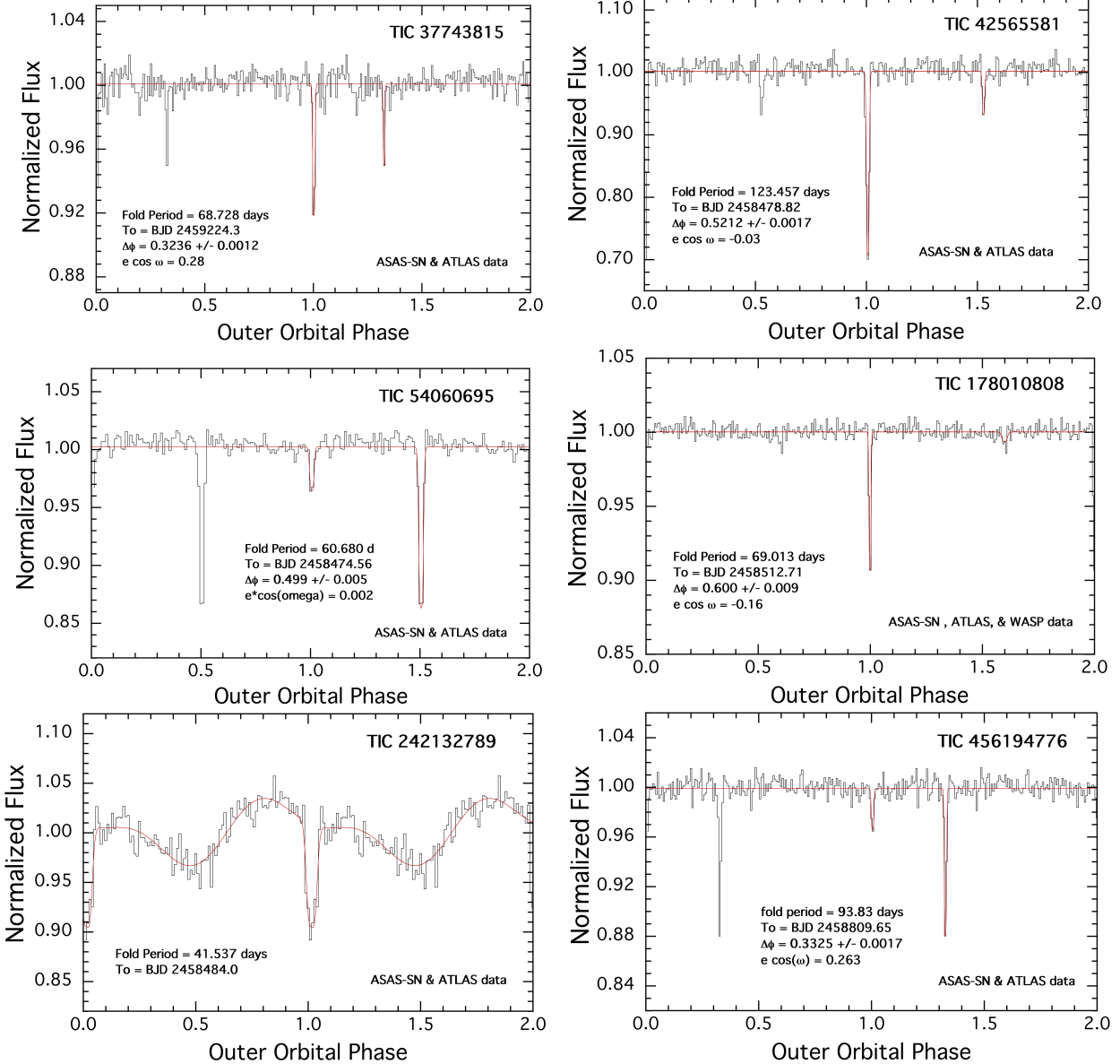


Figure 4. Folded, binned, and averaged lightcurves for the outer orbits of the six triply eclipsing triple stars. These are based on archival data from ATLAS, ASAS-SN, and WASP data (see Sect. 4 for details). On each plot we write the fold period, the epoch reference time of phase zero, the orbital phase difference between the primary and secondary outer eclipses (if both are detected), and the inferred value of $e \cos \omega_{\text{out}}$ based on the fold. The red curve is a fit to the one or two outer eclipses during the second plotted orbital cycle only. These are used to measure the orbital phase difference between the two eclipses and the widths (where possible and appropriate).

of the tertiary, i.e., there are two other stars in the system, though of considerably lower luminosity, we take uncertainties on T_{eff} to be ± 300 K and on R_B to be $\pm 2 R_{\odot}$. Finally, the temperature ratio of the two EB stars can be estimated approximately from the ratio of their eclipse depths.

Using only this limited information, we fit the SED for all the properties of the stars in our six systems. The results are shown in Fig. 2. In each case, the measured SED points (orange circles) have been corrected for interstellar extinction. The continuous green curves represent the model fits for the stars in the EB, while the cyan curve is for the tertiary. The heavier black curve is the total flux from all three stars. One can get a very good sense from these plots just how much the

tertiary dominates the system light. We list on the plots only the nominal best-fitting values for M , R , and T_{eff} for each of the three stars. We do not list the corresponding uncertainties on these parameters here because we employ a more comprehensive photodynamical analysis in Sect. 5 which utilizes the EB and third-body eclipse contributions to the lightcurve, as well as the SED, to determine the final and more accurate stellar parameters. Nonetheless, these first estimates of the stellar parameters provide a very quick estimate of what kinds of stars we are dealing with. The formal uncertainties on the masses are typically 10%. These parameters can then be utilized as the initial input guesses to the photodynamical analysis.

We utilize the system parameters for the stars found from this preliminary SED analysis to show in Fig. 3 the locations of the stars superposed on the MIST evolution tracks. The tertiaries range from ~ 3 to $15 R_{\odot}$, with T_{eff} ranging from 6000 K to 4500 K, respectively. By contrast, most of the binary stars are still on the main sequence, and, with only one exception, range in mass from $1.0\text{--}1.8 M_{\odot}$. Within four of the systems the two EB stars tend to have similar masses.

As a final note on the SED analysis, we point out that we have not considered pre-MS solutions. These are considered and rejected in the photodynamical analysis.

4 OUTER ORBITAL PERIOD DETERMINATION WITH ARCHIVAL DATA

Once we have discovered a triply eclipsing triple system with *TESS*, the most important question to answer after determining the basic parameters of the constituent stars is the nature of its outer orbit, in particular the period and eccentricity. For this purpose, in the absence of RV data, we most often make use of the ASAS-SN (Shappee et al. 2014; Kochanek et al. 2017) and ATLAS (Tonry et al. 2018; Smith et al. 2020) archival data sets. The ASAS-SN data sets typically have $\sim 1500\text{--}3000$ photometric measurements of a given target, while the ATLAS archives often have approximately 1700 photometric measurements. The ATLAS data have the advantage of going somewhat deeper than the ASAS-SN data, but the disadvantage of saturating on brighter stars where ASAS-SN may still perform well. When these two data sets are of comparable quality, we typically add them. Naturally, we also check for KELT (Pepper et al. 2007, 2012), WASP (Pollacco et al. 2006), HAT (Bakos et al. 2002) and MASCARA data (Talens et al. 2017) to see whether they are available for a particular source.

For all the sources, with the exception of TIC 242132789, there were WASP archival data available. We found these to be quite useful in helping to determine the long-term average EB periods. But, it turns out that these data were generally too noisy to aid in the search for the outer third body eclipses, except in the case of TIC 178010808 where the WASP data nicely complemented the ATLAS and ASAS-SN data. For TIC 242132789 there was a set of KELT data in addition to ATLAS and ASAS-SN data. The KELT data marginally detected the spot and ellipsoidal light modulations associated with the outer orbit, but not the outer eclipses.

We do a blind search for the outer eclipses (either outer primary or outer secondary eclipse) using a Box Least Squares transform (Kovács et al. 2002). Before doing the BLS search we remove the lightcurve of the inner EB by Fourier means (as described in Powell et al. 2021). In the process we remove between 5 and 100 orbital harmonics depending on the sharpness of the features in the EB lightcurve. This cleaning process requires knowing the orbital period of the EB very accurately. In turn, we determine the long-term average binary period from the *TESS* data or from the archival data, whichever yield a more precise result.

We show the results of the above procedure for each of our six triply eclipsing triple stars in Fig. 4. In each panel we show a folded, binned, and averaged lightcurve of the archival data about the period corresponding to the largest and most significant peak in the BLS transform. In all cases, the zero

phase for the outer orbit is taken to be the time of one of the third-body eclipses observed in the *TESS* data. In four of the six sources, both the primary and secondary outer eclipses are clearly detected. In those cases, the value of $e \cos \omega_{\text{out}}$ is also accurately determined, in addition to the outer period of the triple. In the fifth source, TIC 178010808, the secondary outer eclipse is only barely detected, if at all. In the sixth source, TIC 242132789, the outer orbital lightcurve has a clear undulating structure superposed on the very clear primary eclipse. Because the slow modulations have the same period as the outer eclipses, we attribute this to starspot(s) on a giant tertiary that is corotating with the binary orbit as well as to ellipsoidal light variations from the giant. Note that the giant in this system has $R \simeq 15 R_{\odot}$. Not only is this star large, but its outer orbital period of 42 days is the shortest among our sample, and one of the shortest period triples known.

5 PHOTODYNAMICAL ANALYSIS FOR THE SYSTEM PARAMETERS

For all six of our triply eclipsing triples, we have carried out a photodynamical analysis with the software package LIGHTCURVEFACTORY (see, e.g. Borkovits et al. 2019a, 2020a, and references therein). As described in earlier work, the code contains (i) a built-in numerical integrator to calculate the three-body perturbed coordinates and velocities of the three stars in the system; (ii) emulators for the *TESS* light curve, the ETVs extracted therefrom, and radial velocity curve (if available), and (iii) an MCMC-based search routine for the system parameters. The latter utilizes an implementation of the generic Metropolis-Hastings algorithm (see e.g. Ford 2005). The use of this software package and the consecutive steps of the entire analysis process have been previously explained in detail as the code was applied to a wide range of multistellar systems (Borkovits et al. 2018, 2019a,b, 2020a,b, 2021; Mitnyan et al. 2020). These included tight and wider triple systems (with and without outer eclipses), as well as quadruple systems with either a 2+2 or 2+1+1 configuration. Here we discuss only a few specific points related to the current triples.

In relatively close systems, as we are studying here, perturbations to the EB orbit and the detailed profiles of the third body eclipses carry important information about the system parameters, including constraints on the masses and orbital elements. However, with only one exception in this current work, we have no RV measurements to help constrain the system parameters. Therefore, we adopt a somewhat different strategy. In the analysis we utilize some a priori knowledge of stellar astrophysics and evolution with the use of PARSEC isochrones and evolutionary tracks (Bressan et al. 2012). We make use of tabulated three-dimensional grids in triplets of {age, metallicity, initial stellar mass} of PARSEC isochrones that have stellar temperatures, radii, surface gravities, luminosities, and magnitudes in different passbands of several photometric systems. Then, we allow the three parameters {age, metallicity, initial stellar mass} to vary as adjustable MCMC variables. The stellar temperature, radius, and actual passband magnitude are calculated through trilinear interpolations from the grid points and these values are used to generate synthetic lightcurves and an SED that can be

Table 3. Orbital and astrophysical parameters of TIC 37743815 and TIC 42565581 from the joint photodynamical *TESS*, ETV, SED and PARSEC isochrone solution. Note that the orbital parameters are instantaneous, osculating orbital elements and are given for epoch t_0 (first row). Therefore, the orbital periods, in particular, cannot be used for predicting the times of future eclipses; see Table 6 for the latter, and Kostov et al. (2021) for a detailed explanation.

	TIC 37743815		TIC 42565581			
	orbital elements					
	subsystem		subsystem			
	Aa–Ab	A–B	Aa–Ab	A–B		
t_0 [BJD - 2400000]	58468.0		58468.0			
P [days]	0.906926 $^{+0.000008}_{-0.000009}$	68.7998 $^{+0.0029}_{-0.0025}$	1.823537 $^{+0.000031}_{-0.000035}$	123.5467 $^{+0.0041}_{-0.0039}$		
a [R_\odot]	4.779 $^{+0.026}_{-0.037}$	105.8 $^{+1.1}_{-0.6}$	9.61 $^{+0.12}_{-0.16}$	187.9 $^{+3.3}_{-2.8}$		
e	0.0093 $^{+0.0065}_{-0.0035}$	0.361 $^{+0.018}_{-0.016}$	0.01227 $^{+0.00041}_{-0.00040}$	0.161 $^{+0.107}_{-0.017}$		
ω [deg]	95.0 $^{+3.6}_{-3.8}$	40.5 $^{+2.8}_{-3.6}$	163.5 $^{+4.3}_{-3.4}$	64 $^{+16}_{-28}$		
i [deg]	89.55 $^{+0.53}_{-0.39}$	89.60 $^{+0.16}_{-0.56}$	90.26 $^{+0.31}_{-0.53}$	89.10 $^{+1.35}_{-0.27}$		
T_0^{inf} [BJD - 2400000]	58469.09761 $^{+0.00014}_{-0.00004}$	58468.2849 $^{+0.0111}_{-0.0096}$	58468.9993 $^{+0.0002}_{-0.0002}$	58479.1476 $^{+0.0076}_{-0.0096}$		
τ [BJD - 2400000]	58486.6584 $^{+0.0092}_{-0.0097}$	58417.24 $^{+0.47}_{-0.61}$	58468.469 $^{+0.022}_{-0.017}$	58405.4 $^{+7.4}_{-16.5}$		
Ω [deg]	0.0	-1.08 $^{+1.92}_{-2.17}$	0.0	4.72 $^{+1.59}_{-9.91}$		
i_m [deg]		1.84 $^{+1.49}_{-0.82}$		5.53 $^{+1.63}_{-1.69}$		
mass ratio [$q = m_{\text{sec}}/m_{\text{pri}}$]	0.642 $^{+0.010}_{-0.010}$	0.905 $^{+0.017}_{-0.053}$	0.997 $^{+0.004}_{-0.004}$	0.638 $^{+0.036}_{-0.014}$		
K_{pri} [km s^{-1}]	104.3 $^{+1.1}_{-1.5}$	39.9 $^{+0.7}_{-2.2}$	132.6 $^{+1.1}_{-1.0}$	30.6 $^{+1.3}_{-0.7}$		
K_{sec} [km s^{-1}]	162.3 $^{+1.3}_{-2.5}$	44.0 $^{+0.4}_{-0.3}$	132.9 $^{+1.2}_{-0.9}$	47.5 $^{+1.7}_{-1.0}$		
	stellar parameters					
	Aa	Ab	B	Aa	Ab	B
	Relative quantities					
fractional radius [R/a]	0.2201 $^{+0.0031}_{-0.0039}$	0.1376 $^{+0.0008}_{-0.0023}$	0.0377 $^{+0.0037}_{-0.0014}$	0.2382 $^{+0.0024}_{-0.0025}$	0.2358 $^{+0.0026}_{-0.0025}$	0.0451 $^{+0.0020}_{-0.0027}$
temperature relative to $(T_{\text{eff}})_{\text{Aa}}$	1	0.7202 $^{+0.0107}_{-0.0094}$	0.9244 $^{+0.0163}_{-0.0362}$	1	1.0001 $^{+0.0007}_{-0.0006}$	0.6959 $^{+0.0204}_{-0.0133}$
fractional flux [in <i>TESS</i> -band]	0.0804 $^{+0.0011}_{-0.0011}$	0.0081 $^{+0.0006}_{-0.0006}$	0.8957 $^{+0.0118}_{-0.0251}$	0.1417 $^{+0.0017}_{-0.0016}$	0.1393 $^{+0.0015}_{-0.0015}$	0.6093 $^{+0.0334}_{-0.0303}$
	Physical Quantities					
m [M_\odot]	1.082 $^{+0.020}_{-0.021}$	0.697 $^{+0.012}_{-0.024}$	1.605 $^{+0.052}_{-0.085}$	1.793 $^{+0.067}_{-0.089}$	1.787 $^{+0.068}_{-0.087}$	2.255 $^{+0.233}_{-0.113}$
R [R_\odot]	1.052 $^{+0.020}_{-0.028}$	0.659 $^{+0.006}_{-0.017}$	4.011 $^{+0.362}_{-0.152}$	2.288 $^{+0.034}_{-0.047}$	2.266 $^{+0.035}_{-0.047}$	8.410 $^{+0.583}_{-0.485}$
T_{eff} [K]	5899 $^{+94}_{-70}$	4255 $^{+112}_{-85}$	5434 $^{+140}_{-210}$	7521 $^{+117}_{-153}$	7521 $^{+119}_{-155}$	5218 $^{+168}_{-130}$
L_{bol} [L_\odot]	1.214 $^{+0.075}_{-0.082}$	0.126 $^{+0.012}_{-0.009}$	12.79 $^{+0.60}_{-0.72}$	15.14 $^{+0.87}_{-1.61}$	14.83 $^{+0.92}_{-1.53}$	47.74 $^{+3.77}_{-3.09}$
M_{bol}	4.56 $^{+0.08}_{-0.07}$	7.02 $^{+0.08}_{-0.10}$	2.00 $^{+0.06}_{-0.05}$	1.82 $^{+0.12}_{-0.06}$	1.84 $^{+0.12}_{-0.07}$	0.57 $^{+0.07}_{-0.08}$
M_V	4.59 $^{+0.08}_{-0.07}$	7.85 $^{+0.18}_{-0.20}$	2.16 $^{+0.07}_{-0.06}$	1.76 $^{+0.14}_{-0.06}$	1.78 $^{+0.13}_{-0.07}$	0.78 $^{+0.08}_{-0.09}$
$\log g$ [dex]	4.427 $^{+0.012}_{-0.009}$	4.644 $^{+0.006}_{-0.002}$	3.438 $^{+0.036}_{-0.090}$	3.969 $^{+0.012}_{-0.010}$	3.976 $^{+0.012}_{-0.010}$	2.935 $^{+0.057}_{-0.030}$
	Global system parameters					
log(age) [dex]		9.384 $^{+0.069}_{-0.021}$		9.044 $^{+0.066}_{-0.059}$		8.935 $^{+0.027}_{-0.089}$
$[M/H]$ [dex]		0.140 $^{+0.122}_{-0.086}$			0.050 $^{+0.145}_{-0.176}$	
$E(B-V)$ [mag]		0.158 $^{+0.047}_{-0.054}$			0.392 $^{+0.051}_{-0.039}$	
extra light ℓ_4 [in <i>TESS</i> -band]		0.016 $^{+0.025}_{-0.012}$			0.110 $^{+0.031}_{-0.034}$	
$(M_V)_{\text{tot}}$		2.04 $^{+0.07}_{-0.06}$			0.13 $^{+0.10}_{-0.06}$	
distance [pc]		1789 $^{+112}_{-55}$			3150 $^{+196}_{-117}$	

compared to their observational counterparts. This process, which is also built into LIGHTCURVEFACTORY, is described in detail in Borkovits et al. (2020a). In our prior work, we have termed these solutions ‘MDN’ (model-dependent-no-RV solutions) which is what we implement here.

Regarding the technical details, in the case of the stellar evolution model dependent runs, the freely adjusted (i.e., trial) parameters were as follows:

(i) Stars: Three stellar masses and the ‘extra light’ contamination, ℓ_4 , from a possible fourth star (or any other con-

taminating sources in the *TESS* aperture). Additionally, the metallicity of the system ($[M/H]$), the (logarithmic) age of the three stars ($\log \tau$), the interstellar reddening $E(B-V)$ toward the given triple, and its distance, were also varied.

(ii) Orbits: Three of six orbital-element related parameters of the inner, and six parameters of the outer orbits, i.e., the components of the eccentricity vectors of the two orbits ($e \sin \omega$)_{in,out}, ($e \cos \omega$)_{in,out}, the inclinations relative to the plane of the sky ($i_{\text{in,out}}$), and moreover, three other parameters for the outer orbit, including the period (P_{out}), time of the first (inferior or superior) conjunction of the tertiary star

Table 4. The same as in Table 3 above, but for TIC 54060695 and TIC 178010808.

	TIC 54060695			TIC 178010808		
	orbital elements					
	subsystem		A–B	subsystem		A–B
	Aa–Ab	B		Aa–Ab	B	
t_0 [BJD - 2400000]	58468.0			58491.5		
P [days]	1.060801 $^{+0.000014}_{-0.000017}$	60.7759 $^{+0.0011}_{-0.0011}$		0.826496 $^{+0.000014}_{-0.000014}$	69.083 $^{+0.022}_{-0.030}$	
a [R_\odot]	5.905 $^{+0.031}_{-0.033}$	107.8 $^{+0.8}_{-0.5}$		5.100 $^{+0.017}_{-0.047}$	114.9 $^{+0.5}_{-1.3}$	
e	0.00211 $^{+0.00096}_{-0.00085}$	0.0154 $^{+0.0090}_{-0.0090}$		0.000026 $^{+0.00014}_{-0.00012}$	0.289 $^{+0.024}_{-0.007}$	
ω [deg]	129 $^{+22}_{-12}$	89.8 $^{+1.8}_{-2.5}$		69 $^{+57}_{-24}$	67.9 $^{+1.3}_{-1.0}$	
i [deg]	89.11 $^{+0.44}_{-0.46}$	88.98 $^{+0.17}_{-0.12}$		86.16 $^{+0.27}_{-0.22}$	88.485 $^{+0.021}_{-0.046}$	
$T_0^{\text{inf/sup}}$ [BJD - 2400000]	58486.6459 $^{+0.0003}_{-0.0003}$	58474.5313 $^{+0.0088^*}_{-0.0088}$		58492.0717 $^{+0.0001}_{-0.0001}$	58512.6976 $^{+0.0023}_{-0.0024}$	
τ [BJD - 2400000]	58486.231 $^{+0.064}_{-0.036}$	58473.6 $^{+29.0}_{-31.5}$		58491.607 $^{+0.116}_{-0.059}$	58510.45 $^{+0.19}_{-0.13}$	
Ω [deg]	0.0	-2.81 $^{+3.52}_{-2.15}$		0.0	-1.84 $^{+0.36}_{-0.29}$	
i_m [deg]	3.20 $^{+1.81}_{-2.36}$			2.95 $^{+0.25}_{-0.26}$		
mass ratio [$q = m_{\text{sec}}/m_{\text{pri}}$]	0.621 $^{+0.005}_{-0.006}$	0.858 $^{+0.011}_{-0.010}$		0.940 $^{+0.003}_{-0.004}$	0.635 $^{+0.004}_{-0.005}$	
K_{pri} [km s^{-1}]	107.8 $^{+0.6}_{-0.7}$	41.5 $^{+0.6}_{-0.3}$		151.0 $^{+0.6}_{-1.4}$	34.1 $^{+0.2}_{-0.2}$	
K_{sec} [km s^{-1}]	173.8 $^{+1.2}_{-1.2}$	48.3 $^{+0.3}_{-0.2}$		160.6 $^{+0.5}_{-1.1}$	53.8 $^{+0.1}_{-0.1}$	
	stellar parameters					
	Aa	Ab	B	Aa	Ab	B
	Relative quantities					
fractional radius [R/a]	0.2744 $^{+0.0017}_{-0.0024}$	0.1426 $^{+0.0013}_{-0.0015}$	0.0774 $^{+0.0009}_{-0.0010}$	0.2994 $^{+0.0014}_{-0.0011}$	0.2642 $^{+0.0016}_{-0.0021}$	0.0249 $^{+0.0017}_{-0.0003}$
temperature relative to (T_{eff}) _{Aa}	1	0.7593 $^{+0.0057}_{-0.0064}$	0.6911 $^{+0.0050}_{-0.0056}$	1	0.9819 $^{+0.0009}_{-0.0009}$	0.9543 $^{+0.0058}_{-0.0368}$
fractional flux [in <i>TESS</i> -band]	0.1070 $^{+0.0008}_{-0.0008}$	0.0122 $^{+0.0003}_{-0.0003}$	0.8396 $^{+0.0270}_{-0.0169}$	0.2008 $^{+0.0027}_{-0.0024}$	0.1482 $^{+0.0014}_{-0.0019}$	0.6340 $^{+0.0084}_{-0.0112}$
	Physical Quantities					
m [M_\odot]	1.513 $^{+0.025}_{-0.027}$	0.939 $^{+0.012}_{-0.015}$	2.099 $^{+0.066}_{-0.032}$	1.341 $^{+0.012}_{-0.035}$	1.261 $^{+0.013}_{-0.035}$	1.650 $^{+0.028}_{-0.060}$
R [R_\odot]	1.622 $^{+0.015}_{-0.022}$	0.842 $^{+0.011}_{-0.013}$	8.345 $^{+0.112}_{-0.119}$	1.526 $^{+0.007}_{-0.008}$	1.348 $^{+0.012}_{-0.019}$	2.859 $^{+0.158}_{-0.036}$
T_{eff} [K]	7358 $^{+151}_{-87}$	5590 $^{+61}_{-48}$	5085 $^{+68}_{-47}$	6331 $^{+198}_{-47}$	6214 $^{+200}_{-43}$	6028 $^{+52}_{-82}$
L_{bol} [L_\odot]	6.838 $^{+0.723}_{-0.329}$	0.618 $^{+0.042}_{-0.029}$	41.62 $^{+2.16}_{-1.17}$	3.369 $^{+0.376}_{-0.093}$	2.447 $^{+0.229}_{-0.063}$	9.772 $^{+0.849}_{-0.261}$
M_{bol}	2.68 $^{+0.05}_{-0.11}$	5.29 $^{+0.05}_{-0.07}$	0.72 $^{+0.03}_{-0.05}$	3.45 $^{+0.03}_{-0.11}$	3.80 $^{+0.03}_{-0.10}$	2.29 $^{+0.03}_{-0.09}$
M_V	2.64 $^{+0.06}_{-0.11}$	5.38 $^{+0.06}_{-0.08}$	0.95 $^{+0.04}_{-0.06}$	3.42 $^{+0.03}_{-0.10}$	3.78 $^{+0.03}_{-0.09}$	2.30 $^{+0.03}_{-0.07}$
$\log g$ [dex]	4.199 $^{+0.006}_{-0.006}$	4.559 $^{+0.007}_{-0.006}$	2.919 $^{+0.010}_{-0.015}$	4.196 $^{+0.003}_{-0.005}$	4.278 $^{+0.005}_{-0.003}$	3.744 $^{+0.012}_{-0.065}$
	Global system parameters					
$\log(\text{age})$ [dex]	9.017 $^{+0.022}_{-0.037}$				9.335 $^{+0.014}_{-0.018}$	
$[M/H]$ [dex]	-0.042 $^{+0.048}_{-0.039}$				0.263 $^{+0.085}_{-0.245}$	
$E(B-V)$ [mag]	0.115 $^{+0.024}_{-0.018}$				0.058 $^{+0.018}_{-0.010}$	
extra light ℓ_4 [in <i>TESS</i> -band]	0.041 $^{+0.017}_{-0.027}$				0.024 $^{+0.019}_{-0.016}$	
$(M_V)_{\text{tot}}$	0.73 $^{+0.04}_{-0.07}$				1.78 $^{+0.02}_{-0.08}$	
distance [pc]	2427 $^{+33}_{-34}$				1415 $^{+35}_{-14}$	

Notes. $T_0^{\text{inf/sup}}$ denotes the moment of an inferior or superior conjunction of the secondary (Ab) and the tertiary (B) along their inner and outer orbits, respectively. Superior conjunctions are noted with *.

observed in the *TESS* data ($T_{\text{out}}^{\text{inf,sup}}$) and, finally, the longitude of the node relative to the inner binary's node (Ω_{out}).

Here we add some additional notes about the ‘age’ and the ‘distance’. First, regarding the ‘age’ parameter, our previous experience has led us to believe that, in some cases, it is better to allow the ages of the three stars to be adjusted individually instead of requiring strict coeval evolution. This issue was briefly discussed in Rowden et al. (2020) and Borkovits et al. (2021), and we discuss it below in the case of some individual sources. Regarding the distance of the triple system, one can argue that the accurate trigonometric distances ob-

tained with Gaia (Bailer-Jones et al. 2021) should be used as Gaussian priors to penalize the model solutions. But, given that neither DR2 nor the recently released eDR3 Gaia parallaxes have been corrected for the multistellar nature of the objects, we consider the published parallaxes and corresponding distances to be not necessarily accurate for our systems. Therefore, we decided not to utilize the Gaia distances. Instead, we constrained the distance by minimizing the χ_{SED}^2 value a posteriori, at the end of each trial step (for results see Sect. 6.1).

A couple of other parameters were *constrained* instead of

Table 5. The same as in Table 3 above, but for TIC 242132789 and TIC 456194776.

	TIC 242132789			TIC 456194776		
	orbital elements					
	subsystem				subsystem	
	Aa–Ab	A–B	Aa–Ab	A–B	Aa–Ab	A–B
t_0 [BJD - 2400000]	58468.0				58790.0	
P [days]	5.1287 $^{+0.0013}_{-0.0013}$	42.0317 $^{+0.0091}_{-0.0085}$	1.7192540 $^{+0.0000071}_{-0.0000075}$		93.915 $^{+0.045}_{-0.038}$	
a [R_\odot]	16.98 $^{+0.13}_{-0.18}$	81.02 $^{+0.68}_{-0.91}$	8.287 $^{+0.019}_{-0.030}$		143.8 $^{+0.4}_{-1.1}$	
e	0.01644 $^{+0.00041}_{-0.00042}$	0.0055 $^{+0.0037}_{-0.0030}$	0.00293 $^{+0.00060}_{-0.00043}$		0.288 $^{+0.040}_{-0.043}$	
ω [deg]	311.4 $^{+2.4}_{-2.3}$	171 $^{+106}_{-51}$	204 $^{+15}_{-9}$		198.9 $^{+2.0}_{-1.8}$	
i [deg]	88.08 $^{+0.47}_{-0.40}$	89.47 $^{+0.14}_{-0.15}$	89.50 $^{+0.39}_{-0.85}$		88.578 $^{+0.035}_{-0.035}$	
$T_0^{\text{inf/sup}}$ [BJD - 2400000]	58470.1198 $^{+0.0011}_{-0.0011}$ *	58484.4801 $^{+0.0054}_{-0.0053}$	58791.5538 $^{+0.0002}_{-0.0003}$		58809.8646 $^{+0.0046}_{-0.0046}$ *	
τ [BJD - 2400000]	58468.163 $^{+0.035}_{-0.033}$	58471.0 $^{+5.0}_{-18.9}$	58791.237 $^{+0.069}_{-0.041}$		58735.9 $^{+1.8}_{-1.3}$	
Ω [deg]	0.0	-0.85 $^{+2.66}_{-0.93}$	0.0		-1.06 $^{+0.71}_{-0.46}$	
i_m [deg]		2.00 $^{+0.88}_{-0.64}$			1.52 $^{+0.40}_{-0.76}$	
mass ratio [$q = m_{\text{sec}}/m_{\text{pri}}$]	0.852 $^{+0.008}_{-0.008}$	0.618 $^{+0.005}_{-0.005}$	0.762 $^{+0.005}_{-0.005}$		0.750 $^{+0.011}_{-0.020}$	
K_{pri} [km s^{-1}]	77.0 $^{+0.7}_{-0.7}$	37.3 $^{+0.4}_{-0.5}$	105.4 $^{+0.5}_{-0.6}$		34.5 $^{+0.4}_{-0.5}$	
K_{sec} [km s^{-1}]	90.4 $^{+0.8}_{-1.1}$	60.3 $^{+0.5}_{-0.6}$	138.4 $^{+0.4}_{-0.5}$		46.1 $^{+0.6}_{-0.6}$	
	stellar parameters					
	Aa	Ab	B	Aa	Ab	B
	Relative quantities					
fractional radius [R/a]	0.1027 $^{+0.0018}_{-0.0018}$	0.0712 $^{+0.0013}_{-0.0012}$	0.1509 $^{+0.0010}_{-0.0010}$	0.1995 $^{+0.0019}_{-0.0017}$	0.1274 $^{+0.0013}_{-0.0013}$	0.0344 $^{+0.0005}_{-0.0005}$
temperature relative to (T_{eff}) _{Aa}	1	0.9658 $^{+0.0085}_{-0.0090}$	0.7170 $^{+0.0102}_{-0.0074}$	1	0.8808 $^{+0.0038}_{-0.0050}$	0.8787 $^{+0.0065}_{-0.0082}$
fractional flux [in <i>TESS</i> -band]	0.0597 $^{+0.0013}_{-0.0013}$	0.0256 $^{+0.0013}_{-0.0010}$	0.8779 $^{+0.0269}_{-0.0279}$	0.1354 $^{+0.0028}_{-0.0028}$	0.0368 $^{+0.0006}_{-0.0005}$	0.8153 $^{+0.0087}_{-0.0230}$
fractional flux [in R_C -band]	—	—	—	0.1399 $^{+0.0058}_{-0.0049}$	0.0362 $^{+0.0012}_{-0.0014}$	0.7944 $^{+0.0181}_{-0.0307}$
	Physical Quantities					
m [M_\odot]	1.346 $^{+0.031}_{-0.045}$	1.146 $^{+0.027}_{-0.034}$	1.539 $^{+0.046}_{-0.060}$	1.464 $^{+0.010}_{-0.015}$	1.115 $^{+0.010}_{-0.014}$	1.939 $^{+0.035}_{-0.056}$
R [R_\odot]	1.741 $^{+0.031}_{-0.030}$	1.207 $^{+0.029}_{-0.027}$	12.22 $^{+0.12}_{-0.13}$	1.653 $^{+0.017}_{-0.017}$	1.055 $^{+0.012}_{-0.013}$	4.940 $^{+0.066}_{-0.084}$
T_{eff} [K]	6568 $^{+101}_{-43}$	6367 $^{+33}_{-66}$	4734 $^{+30}_{-63}$	6709 $^{+263}_{-138}$	5924 $^{+176}_{-114}$	5920 $^{+142}_{-120}$
L_{bol} [L_\odot]	5.118 $^{+0.266}_{-0.262}$	2.135 $^{+0.154}_{-0.135}$	67.27 $^{+1.79}_{-3.34}$	5.059 $^{+0.708}_{-0.505}$	1.245 $^{+0.131}_{-0.117}$	27.12 $^{+2.54}_{-2.54}$
M_{bol}	3.00 $^{+0.06}_{-0.06}$	3.95 $^{+0.07}_{-0.08}$	0.20 $^{+0.06}_{-0.03}$	3.01 $^{+0.11}_{-0.14}$	4.53 $^{+0.11}_{-0.11}$	1.19 $^{+0.13}_{-0.10}$
M_V	2.99 $^{+0.06}_{-0.06}$	3.95 $^{+0.07}_{-0.08}$	0.58 $^{+0.10}_{-0.04}$	2.97 $^{+0.11}_{-0.13}$	4.55 $^{+0.12}_{-0.12}$	1.26 $^{+0.10}_{-0.11}$
$\log g$ [dex]	4.083 $^{+0.017}_{-0.016}$	4.331 $^{+0.012}_{-0.013}$	2.450 $^{+0.007}_{-0.008}$	4.166 $^{+0.007}_{-0.008}$	4.437 $^{+0.008}_{-0.007}$	3.336 $^{+0.013}_{-0.013}$
	Global system parameters					
log(age) [dex]	9.393 $^{+0.040}_{-0.053}$		9.401 $^{+0.023}_{-0.023}$		9.144 $^{+0.021}_{-0.019}$	
$[M/H]$ [dex]		-0.087 $^{+0.072}_{-0.080}$			0.221 $^{+0.089}_{-0.203}$	
$E(B-V)$ [mag]		0.548 $^{+0.013}_{-0.028}$			0.136 $^{+0.051}_{-0.038}$	
extra light ℓ_4 [in <i>TESS</i> -band]		0.036 $^{+0.029}_{-0.026}$ /0.025 $^{+0.019}_{-0.019}$			0.013 $^{+0.024}_{-0.009}$	
extra light ℓ_4 [in R_C -band]		—			0.028 $^{+0.040}_{-0.019}$	
$(M_V)_{\text{tot}}$		0.42 $^{+0.09}_{-0.04}$			1.01 $^{+0.11}_{-0.11}$	
distance [pc]		2667 $^{+28}_{-28}$			1609 $^{+23}_{-24}$	

Notes. $T_0^{\text{inf/sup}}$ denotes the moment of an inferior or superior conjunction of the secondary (Ab) and the tertiary (B) along their inner and outer orbits, respectively. Superior conjunctions are noted with *.

being adjusted or held constant during our analyses. Specifically, the orbital period of the inner binary (P_{in}) and its orbital phase (through the time of an arbitrary primary eclipse or, more strictly, the time of the inferior conjunction of the secondary star – $T_{\text{in}}^{\text{inf}}$) are in this category. They were constrained internally through the ETV curves.

Regarding the atmospheric parameters of the stars, we handled them in a similar manner as in our previous photo-dynamical studies. We utilized a logarithmic limb-darkening law (Klinglesmith & Sobieski 1970) for which the passband-

dependent linear and non-linear coefficients were interpolated in each trial step via the tables from the original version of the **Phoebe** software (Prša & Zwitter 2005). We set the gravity darkening exponents for all late type stars to $\beta = 0.32$ in accordance with the classic model of Lucy (1967) valid for convective stars and hold them constant. For several of our systems, however, the analysis of the net SED has revealed that the EBs contain hotter stars, having radiative envelopes. For these stars, we set $\beta = 1.0$. The choice of this parameter,

however, has only minor consequences, as the stars under the present investigation are close to spheroids.

For the photodynamical analysis we utilized a more sophisticated processing for the *TESS* photometric data by employing the convolution-based differential image analysis tasks of the FITSH package Pál (2012). Furthermore, we note that in preparing the observational data for analysis, to save computational time we dropped out the out-of-eclipse sections of the 30-min cadence *TESS* lightcurves, retaining only the ± 0.15 phase-domain regions around the binary eclipses themselves. However, during sections of the data containing the third-body (i.e., ‘outer’) eclipses, we kept the data for an entire binary period both before and after the first and last contacts of the given third-body eclipse.

Moreover, the mid-eclipse times of the inner binaries, used to define the ETV curves, were calculated in a manner that was described in detail in Borkovits et al. (2016). The ETVs were one of the inputs to the photodynamical analysis. We tabulate all the eclipse times in Appendix C as online only tables.

Finally, note also some system specific departures from the standard procedures described above in the case of two of our triples. These are as follows:

(1) In the case of TIC 242132789, the lightcurve of both *TESS* sectors display non-linear, somewhat erratic variations in the mean out-of-eclipse flux levels. This can partly be attributed to the ellipsoidal light variations (ELV) of the red giant tertiary, which is handled internally by our lightcurve emulator and, therefore, nothing special has to be done to model the ELVs. However, an additional, more erratic contribution to these variations might arise from either time-varying spot activity on the surface of the red giant or any stray light in the aperture (or both). In any case, independent of the origin(s) of this time-varying, irregular contaminating flux, we modelled it by fitting an eighth order polynomial, separately for the two sectors, simultaneously with the triple star lightcurve modelling, during each MCMC step.

(2) The other triple that was handled somewhat differently is TIC 456194776. This system was originally the fourth target of the ground-based photometric follow-up campaign that was described in detail in Sect. 2.3 of Borkovits et al. (2022). In contrast to the other three triply eclipsing triples, of which the detailed analyses were published in Borkovits et al. (2022), unfortunately, we were unable to catch any further third-body eclipses during our observing runs. This is the reason why this system was not included the above-mentioned study, but rather appears in this work. On the other hand, however, we were able to observe 9 regular inner eclipses from the ground between 12 August 2020 and 12 December 2021. Thus, we decided to include these eclipsing lightcurves (in Cousins R_C -band) and also the extracted eclipse times into our analysis. In addition, near the final stages of our analysis we also acquired RV data for this target. Therefore, we carried out a second kind of analysis for this target which we have termed ‘MDR’ (model-dependent-with-RV) with the inclusion of these RV points. We discuss this latter, MDR solution and compare it with the MDN results in Appendix A2. This second type of analysis might also be called a ‘spectro-photodynamical solution’.

6 STELLAR AND ORBITAL PARAMETERS FOR THE SIX TRIPLES

6.1 Individual Triples

In this section we briefly discuss the results for each of the six triply eclipsing triples. When we refer to parameters, they are the ones taken from Tables 3 to 6 based on the photodynamical fits (unless otherwise specifically indicated).

6.1.1 TIC 37743815

The outer period for this system is 68.80 days from the photodynamical solution and 68.72⁴ from the BLS transform of the ASAS-SN and ATLAS data sets. The EB period is 0.9071 d. The quantity $e_{\text{out}} \cos \omega_{\text{out}}$ from a fold of the latter data is 0.28. The photodynamical fit yields $e_{\text{out}} = 0.361$ and $\omega_{\text{out}} = 40.5^\circ$, which combine to give $e_{\text{out}} \cos \omega_{\text{out}} = 0.27$, in excellent agreement with the findings of the archival data. The mutual inclination angle between the inner EB and outer orbit is $1.8^\circ \pm 1^\circ$. The overall system is incredibly flat with i_{in} and i_{out} both within $1/2^\circ$ of 90° .

The mass and radius of the tertiary are $1.6 M_\odot$ and $4.0 R_\odot$, respectively. Both EB stars are considerably lower in mass at $1.1 M_\odot$ and $0.7 M_\odot$. The results from the SED fit (Fig. 2) give the same mass for the tertiary star and a radius that is 12% larger than the photodynamical solution. The primary in the EB has a 16% higher mass from the SED fit than given by the photodynamical fit, while the secondary EB mass is in excellent agreement. In fact, it is instructive to compare the results of the SED fits with those of the more detailed photodynamical results as a type of calibration of the former approach. We mention these comparisons for all the systems.

The distance from the photodynamical fit of 1790 pc is within the uncertainties of 1857 pc given in Table 1. $E(B-V)$ from the photodynamical fit is a bit higher, but significantly so, than the value given in Table 1. We estimate the age of the system as 2.4 Gyr.

6.1.2 TIC 42565581

The outer orbital period of this triple is the longest among our sample of six systems at 123.5 days. This is in excellent agreement with what we found from the archival photometric data. The EB period is 1.8231 days. The system is not exceptionally flat with $i_{\text{mut}} = 5.5^\circ \pm 1.6^\circ$ with the inclination angles of the inner and outer orbits both within a few tenths of a degree of edge on. The eccentricity of the outer orbit is $e_{\text{out}} = 0.16$ with $\omega_{\text{out}} \simeq 61^{+16}_{-28} \text{ deg}$. This combination would be in disagreement with the value of $e_{\text{out}} \cos \omega_{\text{out}} = 0.03$ found from the archival photometric data unless the former value of ω_{out} is near its $1-\sigma$ upper limit of $\sim 77^\circ$.

The tertiary star is the most massive of our sample at $2.2 M_\odot$, and is substantially evolved off the main sequence with $R = 8.4 R_\odot$. The EB stars are near twins with masses of $1.79 M_\odot$, which are much hotter at 7500 K than the tertiary at 5200 K. These are all in satisfactory agreement with the results of our simpler SED fit, except that the mass of the tertiary in the latter fit was about 14% higher, while the EB

⁴ In this section we cite the eclipsing periods, taken from Table 6.

stars were $\sim 20\%$ lower in mass. The radius of the tertiary was the same in both fits.

We find a photometric distance to this source of 3150 pc (with an uncertainty of ~ 150 pc), which agrees well with the Gaia distance of 3180 ± 160 pc. The fitted $E(B - V)$ for this source is 0.39 ± 0.04 compared with the literature tabulated value of only 0.21 ± 0.02 . Finally, we find an age 0.89 ± 0.12 Gyr for the tertiary vs. 1.11 ± 0.15 Gyr for the EB when the two are allowed to have independent ages.

6.1.3 TIC 54060695

The outer period for this system is 60.72 days, in good agreement with the long term mean period of 60.68 days found from the combined archival data of ASAS-SN and ATLAS. The two outer eclipses seen in the outer orbit fold of the archival data yielded an $e \cos \omega_{\text{out}} \simeq 0.002$, while the photodynamical fit yielded separate parameter values of $e_{\text{out}} = 0.015$ and $\omega_{\text{out}} = 89^\circ$. The mutual inclination angle, i_{mut} , between the plane of the inner EB (with period 1.0605 d) and outer orbit is $3^\circ \pm 2^\circ$, while the inclination angles of the individual orbital planes are both close to 89° . These are all consistent with the presence of both a primary and a secondary outer eclipse.

The tertiary star has a mass of $2.1 M_\odot$ and is substantially evolved off the MS with a radius of $8.3 R_\odot$. Its T_{eff} is only 5100 K. The two EB stars are close to 1.5 and $1 M_\odot$, with the primary being considerably hotter at 7350 K. The giant still dominates the system's light with 85% of the luminosity. These values are in decent agreement with those found from the SED fit only (see Fig. 2), but the masses are consistently lower by $\sim 16\%$ in the SED fit.

The photometric distance of 2427 ± 33 pc which is formally 3.4σ farther than the Gaia distance of 2221 ± 50 pc. The fitted value of $E(B - V)$ compares well to the one listed in Table 1. The system has an inferred age of 1.04 Gyr.

6.1.4 TIC 178010808

The outer orbit of TIC 178010808 has a period of 69.02 days, and is also rather flat with $i_{\text{mut}} = 3^\circ \pm 0.3^\circ$, and relatively close to edge on with $i_{\text{in}} = 86^\circ$, and $i_{\text{out}} = 88.5^\circ$. The EB period is 0.8257 days. The eccentricity is characterized by $e_{\text{out}} = 0.29$ with $\omega_{\text{out}} = 68^\circ$. The outer orbit fold using the ASAS-SN, ATLAS, and WASP archival data (see Fig. 4) shows a clear detection of the primary outer eclipse, but there is merely a suggestion of a secondary outer eclipse which is not statistically significant with $e_{\text{out}} \cos \omega_{\text{out}} \simeq 0.16$. This is in substantial disagreement with $e_{\text{out}} \cos \omega_{\text{out}} \simeq 0.1$ found in the photodynamical fit.

All three stars in this system have comparable masses (within $\sim 20\%$ of each other). The tertiary has the largest mass at $1.65 M_\odot$ with a slightly evolved radius of $2.9 R_\odot$. All three stars have $T_{\text{eff}} \simeq 6200 K$. All the stellar parameters are in good agreement with the results of the simple SED fit which employs only minimal constraints, but the SED-fitted radius for the tertiary is about 13% larger at $3.3 R_\odot$. In either case, this is the least evolved tertiary among our set of six triples.

The photodynamic distance of 1415 ± 30 pc is in essentially perfect agreement with the Gaia distance (see Table 1). The

fitted value of $E(B - V)$ is small at 0.058, but in agreement with the value listed in Table 1. Finally, the inferred age of the system is 2.2 Gyr.

6.1.5 TIC 242132789

The outer orbit of TIC 242132789 is the shortest among our set of six triply eclipsing triples at 41.5 days. In that sense it is the most compact of our triples and the fourth shortest period triple system known. It is also, by far the tightest of our systems with a period ratio of $P_{\text{out}}/P_{\text{in}}$ of only 8.2^5 , the second smallest ratio (after KIC 76668648) among all triple stellar systems where both the inner and outer periods are known with sufficient precision. TIC 242132789 is now the tightest known triple with the tertiary being the most massive component. The tertiary in the system is also the largest among our six, with $R = 12.2 \pm 0.1 R_\odot$. This implies that $R_B/a \simeq 0.15$ so perhaps it is not surprising that the outer orbit has nearly circularized with $e_{\text{out}} = 0.006$. The mutual inclination angle is marginally significantly different from zero at $i_{\text{mut}} = 2.0^{+0.9}_{-0.6}$ degrees. The two orbital inclination angles are $i_{\text{in}} = 88.1^\circ$ and $i_{\text{out}} = 89.5^\circ$.

All three stellar components are F stars with the tertiary just higher enough in mass ($1.54 M_\odot$) to have evolved well off the main sequence while the EB primary, at $1.35 M_\odot$ is only slightly evolved. The SED fit is in agreement with these basic facts, but it yields $R_B = 15.6 \pm 1.6 R_\odot$, just barely consistent with the photodynamical analysis, and the primary EB mass is lower by 25% compared to the photodynamical results. Much of this discrepancy may be attributed to the fact that the SED fit yields a distance of 3250 pc, which in excellent agree with Gaia, while the photodynamical solution prefers a much closer distance.

In fact, the photodynamic distance is 2667 ± 28 pc. This is to be compared to the Gaia distance of 3258 ± 165 pc. This is formally a 3.6σ discrepancy, and may partially be accounted for if the Gaia measurement is affected by the EB stars which contribute 10% of the system light. The fitted $E(B - V)$ is close to 0.55, while the value from Table 1 is lower at 0.34. The age of the system is found to be 2.5 Gyr.

This system exhibits the largest ETVs among our sample of triples. The amplitude is 0.01 days with a period of $P_{\text{out}}/2 \simeq 21$ days. The ETV curve for this source is explored further in Appendix A.

6.1.6 TIC 456194776

This system has an outer orbital period of 93.83 days found from the ASAS-SN and ATLAS archival data, which, in turn, is in excellent agreement with the period found from the photodynamical modeling (93.90 days). The EB period is 1.7193 days. The mutual inclination angle between the inner binary and the outer orbit is 1.5° , while i_{in} and i_{out} are 89.5° and 88.6° , respectively. Again, this is a flat and edge on system. The parameter $e \cos \omega_{\text{out}}$ based on the fold of the outer orbit using ASAS-SN and ATLAS data is 0.26. By comparison the individual components from the photodynamical fits are:

⁵ We define the ‘tightness’ of a binary as $P_{\text{out}}/P_{\text{in}}$, where the smaller the ratio, the tighter the binary. In this case, as a technical matter, we use the ratio of periods from Table 3.

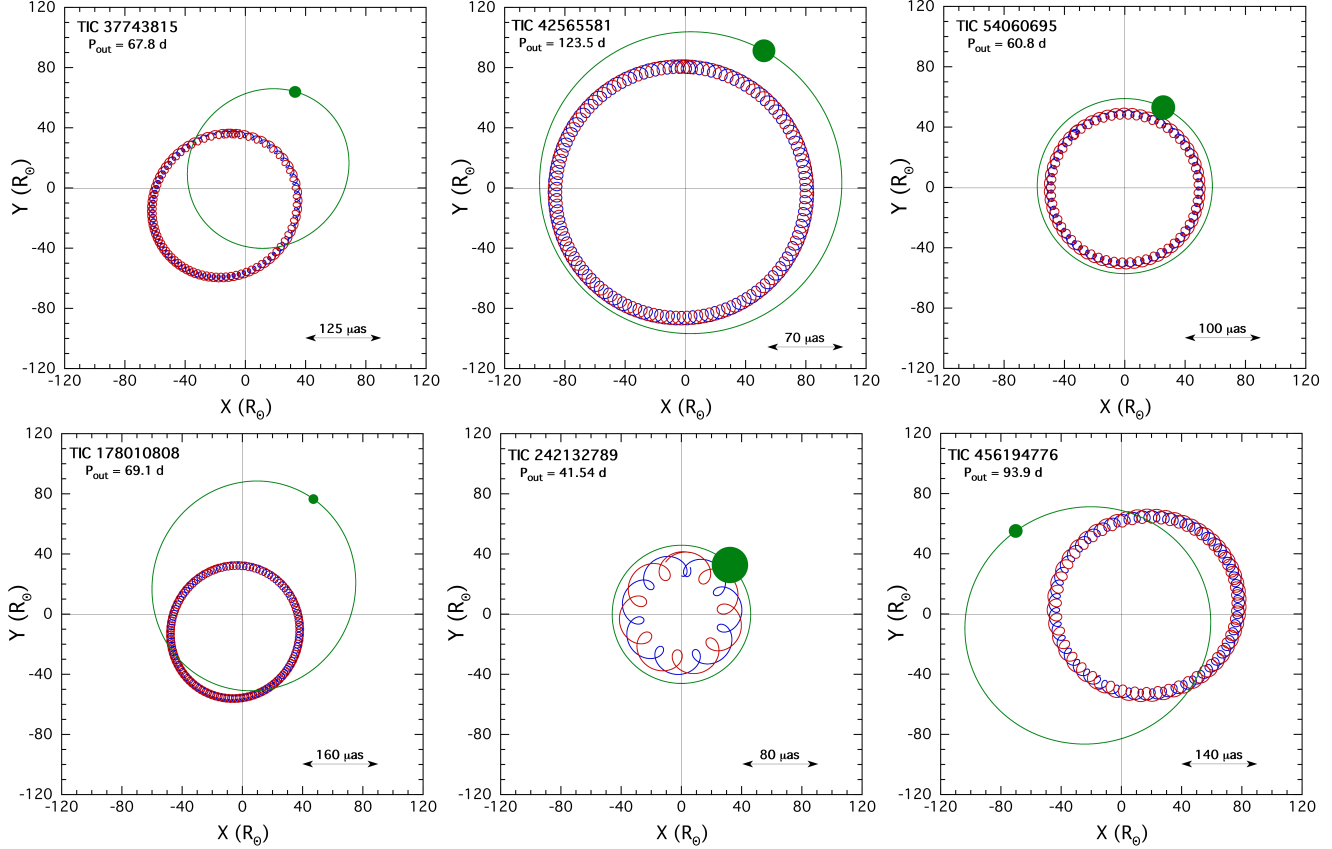


Figure 5. The outer orbits of the six triply eclipsing systems seen from above the orbital plane. The stars are all moving counter-clockwise. The observer is at $y \rightarrow \infty$. Red and blue tracks are for the primary and secondary stars in the EB, respectively, while the green track is that of the tertiary star. The heavy filled green circle represents the size of the tertiary to scale on the plot. Each panel has an angular scale in units of micro-arcseconds. A discussion about how the stellar motions may affect the Gaia distance determinations is given in Appendix B.

$e = 0.29$ and $\omega_{\text{out}} = 199^\circ$, leading to $|e \cos \omega_{\text{out}}| = 0.27$, which is in excellent agreement.

The mass of the tertiary is $1.9 M_\odot$ and its evolved radius is $4.9 R_\odot$. The EB stars are near the main sequence with lower masses of 1.5 and $1.1 R_\odot$. The EB primary is considerably hotter at 6700 K than the evolved tertiary at 5900 K. The SED fit alone yields somewhat hotter EB stars with 16% higher mass, and good agreement with the photodynamical fit for the radius of the tertiary.

The photometric distance of 1609 pc is in excellent agreement with the Gaia value of 1590 pc, given that both uncertainties are of order 30 pc. The fitted photodynamical and MAST values for $E(B-V)$ of 0.14 vs. 0.17 , respectively, are in quite reasonable agreement. The system age is 1.4 Gyr.

This was the one triple system in this work for which we also obtained radial velocity data. We explore in Appendix A2 how the RVs added to the photodynamical solution.

6.2 Common Properties

What all of these six triply eclipsing triple systems have in common is that they are all remarkably flat with i_{mut} within a couple of degrees of zero. In fact, only one of these systems has $i_{\text{mut}} \gtrsim 3^\circ$ and that is TIC 42565581 where $i_{\text{mut}} = 5.5^\circ \pm 1.6^\circ$. The inclination angles of the EB plane and the outer orbit

are all within a few degrees of 90° , and, of course, that is a strong selection effect since we are searching for outer eclipses as a definitive signature of this type of system.

The orbital periods of the six systems are, in order, 41.5 , 60.7 , 68.7 , 69.0 , 93.9 , and 123.5 days. As a measure of how compact these systems are, we note that there are only 8 other triple systems known with comparably short periods (see, e.g., Borkovits et al. 2022). By contrast, only one of our systems is considered ‘tight’, i.e., with a small value of $P_{\text{out}}/P_{\text{in}}$. Specifically, five of the six systems have $P_{\text{out}}/P_{\text{in}}$ in the range of $55\text{--}83$, while TIC 242132789 is unique in this group with a quite small value of $P_{\text{out}}/P_{\text{in}} = 8.2$. This is the second tightest triple known.

Two of the outer orbits of the six triples have notably small eccentricities ($e \lesssim 0.02$). It is interesting that in these two cases, the value of R_B/a_{out} is 0.077 for TIC 54060695 and 0.151 for TIC 242132789. Therefore, it seems likely that tidal circularization may have played a role in the circularization of these systems where the tertiary is both large and substantially convective. For the other four systems, R_B/a_{out} ranges from 0.025 to 0.040 .

The tertiary masses in these systems range from 1.6 to $2.2 M_\odot$, and are all evolved off the main sequence. They have radii between 2.9 and $12 R_\odot$. Their evolutionary ages all range from $1.0\text{--}2.5$ Gyr. The large radii of the tertiary

stars are also something of a selection effect. The probability of outer eclipses in these systems is roughly proportional to R_B/a_{out} . Thus, for similar orbital separations as in these systems (50–100 R_\odot), the outer eclipse probability can be enhanced by nearly an order of magnitude for the size of the tertiaries we have found as compared to when they were on the main sequence.

7 SUMMARY AND DISCUSSION

In this paper we report the discovery and analyses of six triply eclipsing triple systems found from observations with the *TESS* space telescope. They were observed during one to three *TESS* sectors each, yielding precise space-borne photometric data trains. In four cases the source was observed during two sectors, but those sectors were separated by two years. However, when combined with archival ground-based survey photometric measurements (see Fig. 4), we were able to obtain reasonably accurate orbital and stellar parameters for all six triple systems via detailed photodynamical analyses.

This is part of an ongoing program to find and characterize compact triple systems via their signature third-body eclipses. In all we have found 52 such systems during the first three *TESS* cycles. For 20 of these there is sufficient archival data (typically from ASAS-SN and ATLAS, but also including WASP, KELT, and MASCARA) to have determined unambiguously the outer orbit via the long-term detection of third-body eclipses. Generally, with *TESS* we see only one or two third body events because of the sparse coverage, and even when there are two such events, they are sufficiently far apart (i.e., two years), that the outer period is at best ambiguous. There is of course, the additional possibility that even if two eclipses are seen with *TESS*, they are not of the same type, i.e., primary vs. secondary. Of the 20 triply eclipsing triples where we now know the outer period, we have chosen six more of them from this extensive set to report here⁶. This choice of six sources was to strike a balance between being able to discuss each one in some detail, without making the paper too lengthy.

The vast majority of the triply eclipsing systems that we have discovered in the *TESS* data have been found via visual surveys of the lightcurves by the VSG group (Kristiansen et al. 2022). We employ both a machine learning (ML) approach (Powell et al. 2021) and a direct visual search in looking for multistellar systems. Empirically, we have found that the ML approach is superior for finding large numbers of EBs and quadruples within the millions of *TESS* lightcurves, but that the visual approach is substantially more efficient at finding non-repeating, and odd shaped third body eclipses. In all, the VSG has surveyed some 10 million lightcurves while finding 52 with a triply eclipsing triples signature as well as many other interesting and unique phenomena (see Kristiansen et al. 2022). We anticipate that our list of triply eclipsing triples will grow roughly linearly with time as more of the *TESS* lightcurves are inspected.

Most of the definitive determinations of the outer orbital

periods were made using BLS transforms of archival ground-based photometric data sets, after the existence of third-body events was established from the *TESS* data. This raises the question of whether there is a way to find the third body eclipses directly in these archival data sets without first knowing that they are present in a particular source. We are fairly certain that most triple star systems exhibiting eclipses of the tertiary will also contain an eclipsing binary. In that case the dominant source of ‘noise’ in a BLS is from the presence of the much higher duty cycle orbital modulations. In order to detect the third body events in the archival data, it is generally necessary to first subtract out the EB lightcurve. While it is possible to automate such a search and removal operation, it seems more efficient at this point to spot the existence of the third body events first in the precision photometry of the *TESS* data set.

Now that these triply eclipsing triples are known, and their basic parameters determined, more focused follow-up ground-based photometry, especially with small amateur telescopes, would be welcome. All six objects have G magnitudes in the range of 12.2 to 13.5. The ordinary primary eclipse depths range from 2–15%, while the third body eclipses range from a few to 25% deep. The ETV data from *TESS* itself was typically instrumental in determining some of the parameters found from the photodynamical analyses. Thus, future timing observations of the ordinary EB eclipses in these systems would be quite helpful in improving the parameter determinations. The dynamical delays in these systems range from 0.1 to 14 minutes, while the LTTE delays are typically \sim 2 minutes, so readily within the realm of amateur observations. Searches for additional third-body events are difficult without advance approximate predictions since they occur relatively infrequently. In order to facilitate ground-based follow up observations of future third-body events, we provide ephemerides for such observations in Table 6. In some cases, however, these ephemerides are somewhat uncertain, and therefore, we recommend dedicated observations within a wider time domain around each forecasted mid-third-body-eclipse time. Because of the flatness of all these systems, we predict that there will be no eclipse-depth variations either to search for or to cause long ‘outages’ of eclipses.

The six systems discussed in this work are relatively old, of order 1 to a few Gyr. They are manifestly dynamically stable and will last until the tertiary overflows its Roche lobe. In principle, the EB stars could also evolve to mass exchange, but the tertiaries in these systems are sufficiently more massive, and already evolved so that they will fill their Roche lobes, which range in size from 36 to 51 R_\odot , before the EB stars grow by even 10% in size. Generally, once a star of \sim 1.5–2.5 M_\odot has grown to 3–12 times its original radius, we can expect it to fully ascend the giant branch within a small fraction of its total lifetime. These lifetimes are illustrated in Table 7. They also illustrate the fraction of time that systems like these have tertiary stars that are substantially evolved, and hence easier in which to detect third-body eclipses. For example, a 2 M_\odot tertiary that has $R \gtrsim 8 R_\odot$ spends only 37/1350 = 2.7% of its total lifetime in this state.

As mentioned above the VSG group (Kristiansen et al. 2022) has visually examined the lightcurves of some 9 million anonymous *TESS* lightcurves as well as 1 million *TESS* lightcurves of preselected EBs (see Powell et al. 2021; E. Kruse, 2022 in preparation). In all, they have found 52 triply

⁶ Four of the sources from this collection have been reported previously in Borkovits et al. (2020a) and Borkovits et al. (2022).

eclipsing triples with periods in the range of \sim 42–300 days. Thirty two of these were found among the EB lightcurves, and only 20 from among the much more numerous anonymous lightcurves. If each target was observed, on average, during two *TESS* sectors spanning about 50 days, then the probability of finding a third body event in at least one of those sectors is of order 50%, especially when we consider that a fair fraction of the systems exhibit both types of outer eclipses (i.e., primary and secondary). Here we focus on the 32 systems found from among the preselected EB lightcurves. This suggests a ‘success rate’ of 3×10^{-5} per EB. In order to assess the actual fraction of EBs that contain a third body in a compact outer orbit that is coaligned with the inner binary, we use a simple Monte Carlo approach. This takes into account: (i) the probability of seeing a third body eclipse in 50 days of observing; (ii) the fraction of triply eclipsing systems missed because even if the three stars are perfectly aligned it is possible to detect only EB eclipses; and (iii) the detection enhancement because some of the tertiary stars are evolved, i.e., larger than their MS radius. We find that a fraction equal to 2×10^{-4} of all close binaries (period = 0.5 – 20 days) host a third star in a compact 2+1 triple configuration that is flat. Thus, while these are relatively fairly rare systems, there are probably several hundred thousand of them in the Galaxy.

Again, as we have suggested throughout the paper, selection effects favor (i) compact systems, (ii) at least partly flat architecture, and (iii) somewhat evolved tertiaries to enhance the outer eclipse probability. Thus, it is not surprising that these are the systems we have predominantly spotted while surveying the lightcurves.

We have found that the masses of all the stars in the triples we studied are the same to within small factors of order 2. Otherwise the EB might not have been detected in the glare of a much more luminous tertiary. Comparable masses and short outer periods imply an accretion-driven migration formation scenario (see, e.g., Tokovinin 2021 and references therein). In the latter case, the flatness of the systems might demonstrate that such migration is accompanied by orbit alignment. Comparable masses also imply accretion from a common gas source. This mechanism predicts that the outer mass ratio must not exceed unity, and this is indeed the case for the systems presented here. Moderate outer eccentricities as we observe in 4 of the 6 systems can be largely primordial, although circularization by tides in giants also works in some cases (e.g., for TIC 54060695 and TIC 242132789 as we mentioned earlier).

There is also a possible link between our triple systems and 2+2 compact quadruples. Some giants in these triple systems could have originally been second binaries that have merged. This can be revealed by apparent difference of ages, as hinted at in one of our systems: TIC 42565581, though the evidence there is only marginal. These 6 triples with giant tertiaries, favored by observational selection, are also favorable candidates for a triple common envelope phase in the future. In this latter regard, see the studies by (Toonen & Nelemans 2013; Hamers et al. 2022), with emphasis on triple common envelope evolution (Glanz & Perets 2021) and its end products.

Finally, we note that in terms of stellar evolution theory, the tertiary in these systems fixes their age. Thus, we obtain a triplet of reasonably accurate masses and radii with a known age.

DATA AVAILABILITY

The *TESS* data underlying this article were accessed from MAST (Barbara A. Mikulski Archive for Space Telescopes) Portal (<https://mast.stsci.edu/portal/Mashup/Clients/Mast/Portal.html>). The ASAS-SN archival photometric data were accessed from <https://asas-sn.osu.edu/>. The ATLAS archival photometric data were accessed from <https://fallingstar-data.com/forcedphot/queue/>. A part of the data were derived from sources in the public domain as given in the respective footnotes. The derived data generated in this research and the code used for the photodynamical analysis will be shared upon a reasonable request to the corresponding author.

ACKNOWLEDGMENTS

We are grateful to Andrei Tokovinin for going through the manuscript and making some very helpful suggestions for how to interpret our findings.

We thank Allan R. Schmitt and Troy Winarski for making their light curve examining software tools LcTools and AKO-TPF freely available.

VBK is thankful for support from NASA grants 80NSSC21K0351.

TB and ZG acknowledge the support of the Hungarian National Research, Development and Innovation Office (NKFIH) grant K-125015, a PRODEX Experiment Agreement No. 4000137122 between the ELTE Eötvös Loránd University and the European Space Agency (ESA-D/SCI-LE-2021-0025), and the support of the city of Szombathely. ZG acknowledges the Lendület LP2018-7/2021 grant of the Hungarian Academy of Science, the VEGA grant of the Slovak Academy of Sciences No. 2/0031/22, the Slovak Research and Development Agency contract No. APVV-20-0148.

AP acknowledges the financial support of the Hungarian National Research, Development and Innovation Office – NKFIH Grant K-138962.

We thank David Latham for facilitating the TRES observations of TIC 456194776.

The operation of the BRC80 robotic telescope of Baja Astronomical Observatory has been supported by the project “Transient Astrophysical Objects” GINOP 2.3.2-15-2016-00033 of the National Research, Development and Innovation Office (NKFIH), Hungary, funded by the European Union.

This paper includes data collected by the *TESS* mission. Funding for the *TESS* mission is provided by the NASA Science Mission directorate. Some of the data presented in this paper were obtained from the Mikulski Archive for Space Telescopes (MAST). STScI is operated by the Association of Universities for Research in Astronomy, Inc., under NASA contract NAS5-26555. Support for MAST for non-HST data is provided by the NASA Office of Space Science via grant NNX09AF08G and by other grants and contracts.

We have made extensive use of the All-Sky Automated Survey for Supernovae archival photometric data. See Shappee et al. (2014) and Kochanek et al. (2017) for details of the ASAS-SN survey.

We also acknowledge use of the photometric archival data from the Asteroid Terrestrial-impact Last Alert System (ATLAS) project. See Tonry et al. (2018) and Heinze et al. (2018) for specifics of the ATLAS survey.

Table 6. Derived ephemerides for the six triple systems to be used for planning future observations.

TIC ID	37743815	42565581	54060695	178010808	242132789	456194776
Inner binary						
P	0.90707	1.823071	1.06049087	0.8257362	5.11458	1.719349
τ_0	8 469.101	8 469.003	8 486.635	8 492.0725	8 472.69286	8 791.552
A_{ETV}	0.001	0.002	0.001	0.001	0.011	0.007
D	0.105	0.293	0.145	0.155	0.282	0.176
Wide binary (third body eclipses)						
P	68.720	123.452	60.72	69.02:	41.531	93.90:
τ_0^{inf}	9 224.3	8 479.1	8 504.9	8 554.2:	8 484.3	8 841.2:
D^{inf}	1.65	3.23	2.20	0.85:	3.35	1.70:
τ_0^{sup}	9 246.7:	8 543.4:	8 474.51	8 512.75	8 505.3	8 809.90
D^{sup}	1.05:	2.30:	1.95	1.00	3.35	1.90

Notes. (a) For the inner pairs: P , τ_0 , A_{ETV} , D are the period, reference time of a primary minimum, half-amplitude of the ETV curve, and the full duration of an eclipse, respectively. τ_0 is given in BJD – 2 450 000, while the other quantities are in days. As all the inner eccentricities are very small and, hence, the shifts of the secondary eclipses relative to phase 0.5 are negligible (quantitatively, they are much smaller than the full durations of the individual eclipses), the same reference times and periods can be used to predict the times of the secondary eclipses. (b) For the outer orbits we give separate reference times for the third body eclipses around the inferior and superior conjunctions of the tertiary component. The eclipse durations, D , of the third-body eclipses do not give the extent of any specific third body events. Rather D represents the time difference corresponding to the very first and last moments around a given third-body conjunction when the first/last contact of a third-body event may occur). Double dots (:) (1) at the outer periods of TICs 178010808 and 456194776 refer to larger uncertainties arising from the fact that in these two triples only one third-body eclipse was observed with *TESS*; (2) at superior/inferior conjunction times refer to those kinds of third-body events (i.e., primary vs. secondary outer eclipses) that were not observed with *TESS*. For these events, the ephemerides are based on the archival data folds (see Fig. 4), and they might be less certain.

Table 7. Evolution Times in Myr of the Tertiary Stars

Phase	$1.5 M_\odot$	$2.0 M_\odot$	$2.5 M_\odot$
$3.0 R_\odot \rightarrow$ tip of RGB	247	61	13
$8.0 R_\odot \rightarrow$ tip of RGB	86	37	8
$15 R_\odot \rightarrow$ tip of RGB	28	26	4
giant \rightarrow AGB	126	300	200
total evolution	2900	1350	780

Notes. All times were computed with the **MESA** stellar evolution code. $2.5 M_\odot$ stars will not attain sufficiently large radii to fill their Roche lobes during the ascent of the RGB in the systems under discussion.

This work has made use of data from the European Space Agency (ESA) mission *Gaia*⁷, processed by the *Gaia* Data Processing and Analysis Consortium (DPAC)⁸. Funding for the DPAC has been provided by national institutions, in particular the institutions participating in the *Gaia* Multilateral Agreement.

This publication makes use of data products from the Wide-field Infrared Survey Explorer, which is a joint project of the University of California, Los Angeles, and the Jet Propulsion Laboratory/California Institute of Technology, funded by the National Aeronautics and Space Administration.

This work also makes use of data products from the Two Micron All Sky Survey, which is a joint project of the University of Massachusetts and the Infrared Processing and Anal-

ysis Center/California Institute of Technology, funded by the National Aeronautics and Space Administration and the National Science Foundation.

We used the Simbad service operated by the Centre des Données Stellaires (Strasbourg, France) and the ESO Science Archive Facility services (data obtained under request number 396301).

REFERENCES

- Alonso R., Deeg H. J., Hoyer S., Lodieu N., Palle E., Sanchis-Ojeda R., 2015, *A&A*, 584, L8
- Bailer-Jones, C. A. L., Rybizki, J., Fouesneau, M., Demleitner, M., Andrae, R., 2021, *AJ*, 161, 147
- Bakos, G., Á., Lázár, J., Papp, I., Sári, P., Green, E. M., 2002, *PASP*, 114, 974
- Bianchi, L., Shiao, B., & Thilker, D. 2017, *ApJS*, 230, 24
- Borkovits, T., Érdi, B., Forgács-Dajka, E., Kovács, T., 2003, *A&A*, 398, 1091
- Borkovits, T., Derekas, A., Kiss, L. L., et al., 2013, *MNRAS*, 428, 1656
- Borkovits, T., Rappaport, S., Hajdu, T., Sztakovics, J., 2015, *MNRAS*, 448, 946
- Borkovits, T., Hajdu, T., Sztakovics, J., Rappaport, S., Levine, A., Bíró, I. B., Klagyivik, P., 2016, *MNRAS*, 455, 4136
- Borkovits, T., Albrecht, S., Rappaport, S., et al. 2018, *MNRAS*, 478, 513
- Borkovits, T., Rappaport, S., Kaye, T., et al. 2019a, *MNRAS*, 483, 1934
- Borkovits, T., Sperauskas, J., Tokovinin, A., Latham, D. W., Csányi, I., Hajdu, T., Molnár, L., 2019b, *MNRAS*, 487, 4631
- Borkovits, T., Rappaport, S., Hajdu, T., et al. 2020a, *MNRAS*, 493, 5005
- Borkovits, T., Rappaport, S., Tan, T.G., et al. 2020b, *MNRAS*, 496, 4624

⁷ <https://www.cosmos.esa.int/gaia>

⁸ <https://www.cosmos.esa.int/web/gaia/dpac/consortium>

- Borkovits, T., Rappaport, S., Maxted, P. F. L., et al. 2021, MNRAS, 503, 3759
- Borkovits, T., Mitnyan, T., Rappaport, S., et al. 2022, MNRAS, 510, 135
- Borkovits, T. 2022, ‘Eclipsing Binaries in Dynamically Interacting Close, Multiple Systems’, Galaxies, 10, 9 (arXiv:2201.01243)
- Borucki W. J. et al., 2010, Science, 327, 977
- Bouma, L., Hartman, J., Bhatti, W. 2019, ApJS, 245, 13.
- Bressan, A., Marigo, P., Girardi, L. et al. 2012, MNRAS, 427, 127
- Buchhave, L.A., Bakos, G. A., Hartman, J.D., et al. 2010, ApJ, 720, 1118, doi: 10.1088/0004-637X/720/2/1118
- Carter, J.A., et al., 2011, Science, 331, 562
- Castelli F., Kurucz R. L., 2003, in Piskunov, N., Weiss, W.W., Gray D. F., eds, Proc. IAU Symp. 210, Modelling of Stellar Atmospheres. p.A20, preprint (astro-ph/0405087)
- Chambers, K.C., Magnier, E.A., Metcalfe, N., et al. 2016, arXiv:1612.05560
- Choi J., Dotter A., Conroy C., Cantiello M., Paxton B., & Johnson B. D., 2016, ApJ, 823, 102
- Cutri, R.M., Wright, E.L., Conrow, T., et al. 2013, wise.rept, 1C.
- Donati, J.-F., Semel, M., Carter, B. D., Rees, D. E., & Collier Cameron, A. 1997, MNRAS, 291, 658, doi: 10.1093/mnras/291.4.658
- Dotter A., 2016, ApJS, 222, 8
- Fausnaugh, M.M., Burke, C.J., Ricker, G.R., & Vanderspek, R. 2020, Research Notes of the AAS, 4, 251
- Ford, E. B., 2005, AJ, 129, 1706
- Gaia Collaboration, Brown, A. G. A., Vallenari, A., Prusti, T. et al. 2021, A&A, 649, A1
- Furesz, G. 2008, PhD thesis, University of Szeged
- Glanz, H., & Perets, H.B. 2021, MNRAS, 500, 1921
- Green, G.M., Schlafly, E.F., Zucker, C., Speagle, J.S., & Finkbeiner, D.P. 2019, arXiv:1905.02734
- Gunn, J.E., Carr, M., Rockosi, C., et al. 1998, AJ, 116, 3040
- Hammers, A.S., Perets, H.B., Thompson, T.A., & Neunteufel, P. 2022, ApJ, 925, 178
- Heinze, A.N., Tonry, J.L., Denneau, L., et al. 2018, AJ, 156, 241
- Henden, A. A., Levine, S., Terrell, D., Welch, D. 2015, American Astronomical Society, AAS Meeting #225, id.336.16
- Howell, S.B., Sobeck, C., Hass, M., et al. 2014, PASP, 126, 398
- Huang, C.X., Vanderburg, A., Pál, A., et al., 2020, RNAAS, 4, 206
- Jenkins, J.M., Twicken, J.D., McCauliff, S., et al. 2016, in: Software and Cyberinfrastructure for Astronomy IV, volume 9913. International Society for Optics and Photonics, p. 99133E
- Klinglesmith, D. A., Sobieski, S., 1970, AJ, 75, 175
- Kochanek, C. S., Shappee, B. J., Stanek, K. Z., et al., 2017, PASP, 129, 104502
- Kostov et al., 2021, ApJ, 917, 93
- Kostov, V.B., Powell, B.P., Rappaport, S.A., et al. 2022, ApJS in press, arXiv:2202.05790
- Kovács, G., Zucker, S., Mazeh, T., 2002, A&A, 391, 369
- Kozai, Y. 1962, AJ, 67, 591
- Kristiansen, M.H., Rappaport, S., Vanderburg, A., et al. 2022, submitted to PASP.
- Latham, D. W., Stefanik, R. P., Torres, G., et al. 2002, AJ, 124, 1144
- Lidov, M. L., 1962, Planetary and Space Science, 9, 719
- Lucy, L.B. 1967, Zeitschrift für Astrophysik, 65, 89
- Masuda, K., Uehara, S., Kawahara, H. 2015, ApJ, 806, L37
- Mitnyan, T., Borkovits, T., Rappaport, S., Pál, A., Maxted, P. F. L., 2020, MNRAS, 498, 6034
- Nardiello, D., Borsato, L., Piotto, G., et al. 2019, NNRAS, 490, 3806
- Nordström, B., Latham, D. W., Morse, J. A., et al. 1994, A&A, 287, 338
- Ochsenbein, F., Bauer, P., & Marcout, J. 2000, A&AS, 143, 23
- Oelkers, R.J., & Stassun, K.G. 2018, AJ, 156, 132
- Orosz, J., 2015, ASPC, 496, 55
- Paegert, M. et al, 2021, arXiv:2108.04778
- Pál, A., 2012, MNRAS, 421, 1825
- Paxton, B., Bildsten L., Dotter A., Herwig F., Lesaffre P., & Timmes F., 2011, ApJS, 192, 3
- Paxton, B., et al., 2015, ApJS, 220, 15
- Paxton, B., et al., 2019, ApJS, 243, 10
- Pepper, J., Pogge, R.W., DePoy, D.L., et al., 2007, PASP, 119, 923
- Pepper, J., Kuhn, R.B., Siverd, R., et al., 2012, PASP, 124, 230
- Pollacco, D. L., Skillen, I., Collier Cameron, A., et al. 2006, PASP, 118, 1407
- Powell, B.P., Kostov, V.B., Rappaport, S., et al. 2021, AJ, 161, 162
- Prša, A., & Zwitter, T., 2005, ApJ, 628, 426
- Rappaport, S., Kurtz, D., Handler, G., et al. 2021, MNRAS, 503, 254
- Ricker, G.R., Winn, J.N., Vanderspek, R., et al. 2015, JATIS, 1, 014003
- Rowden, P., et al., 2020, AJ, 160, 76
- Schmitt, A.R., Hartman, J.D., & Kipping, D.M. 2019, arXiv:1910.08034
- Shappee, B. J., Prieto, J. L., Grupe, D., et al. 2014, ApJ, 788, 48
- Skrutskie, M.F., Cutri, R.M., Stiening, R., et al. 2006, AJ, 131, 1163
- Smith, K.W., Smartt, S.J., Young, D.R., Tonry, J.L., et al. 2020, PASP, 132, 5002.
- Talens, G.J.J., Spronck, J.F.P., Lesage, A.-L., Otten, G.P.P.L., Stuik, R., Pollacco, D. & Snellen, I.A.G. 2017, A&A, 601, A11
- Tokovinin, A., 2021, Universe, 7, 352
- Toonen, S., & Nelemans, G. 2013, A&A, 557, 87
- Tonry, J.L., Denneau, L., Heinze, A.N., et al. 2018, PASP, 130, 4505
- von Zeipel, 1910, AN, 183, 345
- Wolf, C., Onken, C.A., Luvaal, L.C., et al. 2018, PASA, 35, 10

APPENDIX A: SUPPLEMENTARY MATERIAL – RV AND ETV FITS

A1 Interpretation of the large amplitude ETV of TIC 242132789

As was mentioned in Sect. 5, the analysis of the ETV curves that are extracted from the high-precision *TESS* lightcurves are inherent in our photodynamical analyses. They provide very strict constraints on the eclipsing periods of the inner EBs and, in the case of some eccentricities, the parameters $e_{\text{in}} \cos \omega_{\text{in}}$ are also very strictly constrained through these data. In the case of five of the six investigated systems, however, due to the very short durations of the *TESS* observations, the ETV curves do not carry any useful information about the outer orbits nor, therefore, on the system configurations. The only exception is the ETV curve of TIC 242132789 which exhibits large amplitude ($\mathcal{A}_{\text{ETV}} \sim 0^{\text{d}}.01$), quasi-sinusoidal variations with a period which is exactly half of the outer orbital period, P_{out} (see Fig. A1). Here we briefly discuss the origin of this timing variation, and its implications for the analytic perturbation theories of hierarchical triple systems.

First, it is evident that this ETV cannot arise from the well-known geometric light-travel time effect (LTTE), for at least three reasons. (1) The LTTE has the same period as the outer period. (2) Since in this system the outer orbit is found to be almost circular, the third-body eclipses should have occurred at the extrema of an LTTE generated ETV curve, while, as is seen in Fig. A1, the *TESS*-observed third-body

events occurred approximately mid-way between the two extrema. Finally (3), with the use of the masses and orbital elements found from the photodynamical analysis (Table 5) one can calculate the expected amplitude of the LTTE as being $\mathcal{A}_{\text{LTTE}} \sim 10^{-3}$ d, i.e., one order of magnitude smaller than is observed.

Second, it is also clear that the ETV cannot be the consequence of the usually considered medium period class perturbations of the tertiary.⁹ It was shown by Borkovits et al. (2003) that in a coplanar, doubly circular hierarchical triple system (like TIC 242132789) the largest amplitude, quadruple-order perturbations disappear. This finding was confirmed later with the analyses of the recently discovered, doubly circular, coplanar, triply eclipsing triple systems such as HD 181068 (Borkovits et al. 2013), TIC 278825952 (Mitsyan et al. 2020), and TIC 193993801 (Borkovits et al. 2022). Moreover, though it was found by Borkovits et al. (2015) that the octuple-order perturbation terms do not vanish for such a scenario, their characteristic periods are P_{out} and/or $P_{\text{out}}/3$, but not the half of the orbital period.

On the other hand, as was also discussed in Borkovits et al. (2015), for the tightest triple systems the strict hierarchical approximation no longer remains fully valid. This fact makes it necessary to include some further terms that are denoted as ‘ P_{out} time-scale residuals of the P_{in} time-scale dynamical effects’. According to their calculations (Eqs. 20 and 21), the leading term of this expression for a doubly circular, coplanar configuration gives the following ETV contribution:

$$\Delta_{\text{short}} = \frac{11}{16\pi} \frac{m_B}{m_{AB}} \frac{P_{\text{in}}^3}{P_{\text{out}}^2} \sin \left[2 \frac{2\pi}{P_{\text{out}}} \left(t - \mathcal{T}_{\text{out}}^{\text{inf}} \right) \right]. \quad (\text{A1})$$

Substituting the third-body (m_B) and the total system (m_{AB}) masses, as well as the inner and outer periods ($P_{\text{in,out}}$) from Table 5, one readily finds for the amplitude that $\mathcal{A}_{\text{short}} = 0.0064$, which is close to the observed value. Moreover, the expression above describes well not only the amplitude and period of the observed ETV, but also its phase. And, according to Eq. (A1), both kinds of third-body eclipses should occur mid-way between the lower and upper extrema of the ETV curve, as is very nicely demonstrated in Fig. A1. Therefore, we may conclude that the large amplitude ETV in the case of TIC 242132789 originates from this latter effect. On the other hand, the fact that the theoretically computed amplitude is only about two thirds of the observed value, may serve as cautionary note. And, some further more sophisticated theoretical modeling may be worthwhile for the correct analytical description of the \sim month-timescale perturbations of the tightest triple star systems.

A2 A more in-depth analysis of TIC 456194776, including ground based RV data

Late in the production of this paper, we were fortunate enough to acquire a significant number of radial velocity measurements of this target. We obtained spectroscopic observa-

⁹ In hierarchical triple systems the periodic perturbations have three different classes, according to their characteristic time-scales, as (i) short period ones with characteristic time-scale of P_{in} , (ii) medium period ones, having time-scale of P_{out} , and (iii) long period perturbations, which are effective on a time-scale of $P_{\text{out}}^2/P_{\text{in}}$.

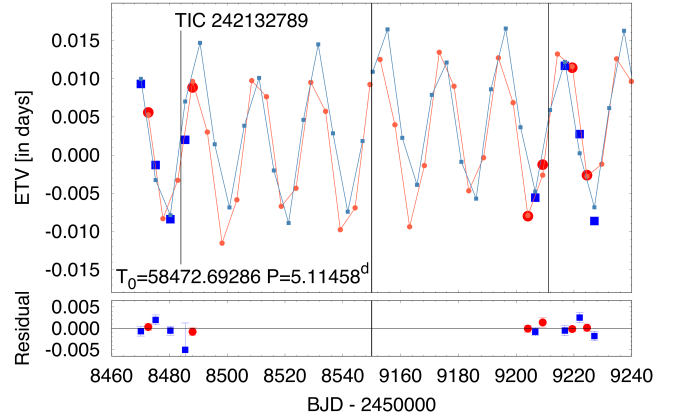


Figure A1. Photodynamical fit to the *TESS* ETV curves for TIC 242132789. Note the high amplitude of the ETVs and the fact that they oscillate at twice the frequency of the outer orbit (i.e., every \sim 21 days.) The larger and darker red circles and blue squares represent the observed primary and secondary times of EB eclipses, while the smaller, lighter symbols, connected with straight lines are taken from the photodynamical model ETV curve. The two thin vertical lines denote the locations of the two third-body outer eclipses. Residuals are also shown in the lower panel, where the uncertainty on each point is also noted.

tions of the target TIC 456194776 with the Tillinghast Reflector Echelle Spectrograph (TRES, Furesz 2008), on the 1.5-m reflector at the Fred Lawrence Whipple Observatory (FLWO) in Arizona, USA. TRES is a high-resolution fiber-fed echelle spectrograph, with a spectral resolving power of $R = 44000$ over the wavelength region of 3900–9100 Å. A total of 20 observations were obtained of TIC 456194776 between Sept 21, 2021 and Jan 26, 2022, with signal-to-noise ratios per resolution element of 23–40 in the Mg b triplet wavelength region (\sim 5187 Å). The spectra were extracted and reduced as per Buchhave et al. (2010), with wavelength solutions derived from bracketing Th-Ar lamp exposures. Visual inspection of the spectra revealed only the lines of the brighter tertiary (star B). Radial velocities were derived by cross-correlation against a suitable synthetic template from a large pre-computed library based on model atmospheres by R. L. Kurucz, and a line list tuned to better match real stars (see Nordström et al. 1994; Latham et al. 2002). These templates cover a limited wavelength region near the Mg b triplet. We find the tertiary to be a rapidly rotating star with an estimated $v \sin i$ of about 80 km s⁻¹.

The 20 radial velocities and their uncertainties are given in Table A1, while the RV points are plotted in Fig. A2. The solid blue curve is the photodynamical fit that was produced during the analysis that led up to the MDR (model-dependent-with-RVs) solution discussed in Sect. 5.

In Table A2 we compare the photodynamical fits for TIC 456194776 using both the MDN and MDR models. Recall that in the latter we add the RV points to the analysis in addition to the photometry, ETV points, SED data, and the use of stellar evolution tracks and model atmospheres. Of all the parameters that we compute, we limit the ones that are compared in the Table to only 5 orbital, 3 stellar, and 2 global system parameters, as illustrative and representative. This comparison serves as a direct ‘calibration’ as to how

Table A1. Measured radial velocities of the tertiary component of TIC 456194776. The date is given as BJD – 2 450 000, while the RVs and their uncertainties are in km s^{-1} .

Date	RV _B	σ_{B}	Date	RV _B	σ_{B}
9478.950099	-57.49	1.70	9527.793497	29.48	4.65
9488.905299	-49.90	3.77	9531.733497	20.00	1.69
9493.853498	-26.85	2.08	9534.827997	25.57	3.51
9497.825098	-12.50	2.92	9546.797096	12.98	2.88
9504.781298	17.93	2.34	9557.734596	-2.03	2.48
9507.755898	15.05	1.62	9567.663896	-36.08	2.18
9514.843597	31.94	3.20	9582.678395	-52.31	2.10
9519.872897	26.39	2.15	9591.693095	-22.35	1.94
9521.876697	32.75	2.31	9596.620294	-1.33	2.62
9524.771097	23.14	2.26	9605.728294	15.71	1.51

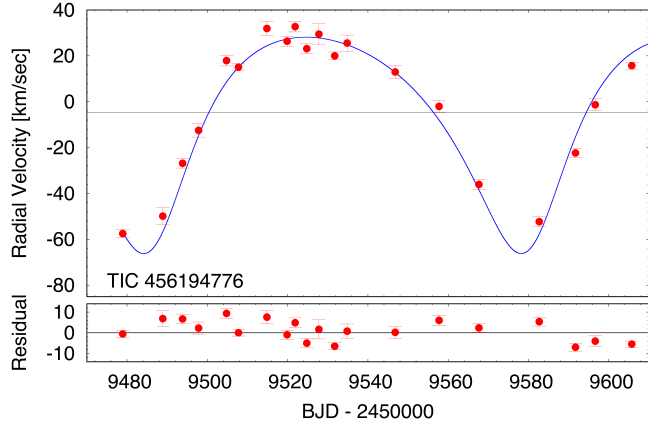


Figure A2. Photodynamical fit to the 20 TRES radial velocity data points for TIC 456194776. The RVs points with uncertainties are given in Table A1. The blue curve is from the spectro-photodynamical analysis described in Sect. 5.

well we can do without the RVs. All of the stellar and global parameters agree to within 1 mutual σ of the two solutions. Likewise, among the orbital elements, the a , i , and Ω values agree to within just somewhat more than 1 σ . The two most interesting differences are in ω_{in} and the eccentricities. In particular the two models differ in e_{in} by 1.7 σ . For e_{out} , where the RV data points help most directly, the two model values differ by only 1/2 σ . We see that the two values of ω_{in} differ by 1.7 σ . Thus, overall, we find the models with and without the use of RVs to be in quite substantial agreement. Finally, it is interesting to note, but hardly surprising, that the one parameter where the error bars shrank considerably is for the outer eccentricity.

Table A2. TIC 456194776: Abbreviated Parameter Comparison Between MDR and MDN Models

	MDR		MDN	
	orbital elements			
	subsystem		subsystem	
	Aa–Ab	A–B	Aa–Ab	A–B
a [R_\odot]	$8.282^{+0.021}_{-0.029}$	$143.5^{+0.49}_{-0.32}$	$8.287^{+0.019}_{-0.030}$	$143.8^{+0.4}_{-1.1}$
e	$0.00437^{+0.00058}_{-0.00057}$	$0.314^{+0.011}_{-0.010}$	$0.00293^{+0.00060}_{-0.00043}$	$0.288^{+0.040}_{-0.043}$
ω [deg]	$231.3^{+4.9}_{-5.6}$	$197.2^{+1.3}_{-1.5}$	204^{+15}_{-9}	$198.9^{+2.0}_{-1.8}$
i [deg]	$88.36^{+0.28}_{-0.63}$	$88.544^{+0.038}_{-0.042}$	$89.50^{+0.39}_{-0.85}$	$88.578^{+0.035}_{-0.035}$
Ω [deg]	0.0	$0.24^{+0.50}_{-0.41}$	0.0	$-1.06^{+0.71}_{-0.46}$
γ [km s^{-1}]		$-4.93^{+0.21}_{-0.20}$	—	
	stellar parameters			
	Aa	Ab	B	Aa
	Physical Quantities			
m [M_\odot]	$1.468^{+0.011}_{-0.013}$	$1.106^{+0.011}_{-0.014}$	$1.913^{+0.026}_{-0.028}$	$1.464^{+0.010}_{-0.015}$
R [R_\odot]	$1.666^{+0.017}_{-0.022}$	$1.047^{+0.018}_{-0.014}$	$4.947^{+0.085}_{-0.072}$	$1.653^{+0.017}_{-0.017}$
T_{eff} [K]	6870^{+191}_{-123}	6004^{+158}_{-93}	5944^{+168}_{-72}	6709^{+263}_{-138}
	Global system parameters			
log(age) [dex]		$9.141^{+0.007}_{-0.015}$		$9.144^{+0.021}_{-0.019}$
distance [pc]		1609^{+33}_{-25}		1609^{+23}_{-24}

APPENDIX B: CLOSER LOOK AT THE DISTANCES

Here we attempt to compute the contribution to the uncertainty in Gaia’s parallax measurement due to the motion of the triple’s center of light (‘col’) as the stars move around in their orbits. Since all three stars are completely unresolved by Gaia’s optics, we consider only the motion of the center of light around the triple’s center of mass. We treat the inner eclipsing binary as a single point source of light, and the tertiary as a second displaced light source in the system. The location of the center of light is taken simply to be:

$$\vec{r}_{\text{col}}(t) = \frac{\mathcal{R}_B(t)L_B - \mathcal{R}_A(t)L_A}{L_A + L_B} \hat{r} \quad (\text{B1})$$

$$= \frac{(M_A L_B - M_B L_A)}{(M_A + M_B)(L_A + L_B)} \mathcal{R}(t) \hat{r} \quad (\text{B2})$$

where $\mathcal{R}_B(t)$ and $\mathcal{R}_A(t)$ are the distances from the triple’s center of mass to the tertiary star (B) and binary (A, center of mass), respectively, L_B and L_A are the luminosity of the tertiary and of the inner binary, respectively, and similarly for the masses M_B and M_A . For simplicity, here we consider only the bolometric luminosities. The vector \hat{r} is the unit vector pointing from the system center of mass to the tertiary star, and projected onto the plane of the sky. In turn, $\vec{\mathcal{R}}(t) \equiv \mathcal{R}(t)\hat{r}$ describes the ordinary Keplerian motion of the outer orbit of the triple system. The masses, luminosities, and orbital parameters are given in Tables 3, 4, and 5.

For each of our six triples, we used this prescription to compute the semi-major axis of the center of light as it orbits the center of mass of the triple system. To generate the motion on the sky as a function of time, we used the orbital parameters for the triples given in the Tables listed above. Because the orbits of all the triples are practically flat, and viewed nearly edge on, we simply took the motion to lie along a line on the sky. We do not know the position angle of the orbit projected on the plane of the sky, and so we used an illustrative angle of 45° , though after trying several different angles we realized the fact that our results are completely independent of this choice.

In Table B1 we give in columns 5, 6, and 7, the size of the semi-major axis of the center of light in micro-arcseconds, the rms deviation from the parallactic ellipse that the orbit produces, and the error that this is likely to introduce into Gaia’s measurement of the parallax. For the latter we simply use the rms deviation divided by the square root of the number of measurements Gaia makes over the 34 month duration of the Gaia eDR3 data set minus the number of astrometric fitted parameters (6). The number of measurements is listed in the last column of Table B1 as astrometric_matched_transits. We note, though, that the exact value of the distance uncertainty introduced by the motion of the center of light is also dependent on how the Gaia sampling (every few weeks) ‘beats’ up with the outer orbital period of the triple¹⁰.

The first four columns of Table B1 are the TIC number of the triple system, the distance determined in this work as part of the photodynamical solution, the distance determined by Gaia, and the cited uncertainty in Gaia’s parallax. Columns 8, 9, and 10 in Table B1 are several Gaia measures of how well

the astrometric solution fits the observations. The parameter ϵ_i is the astrometric excess noise, which Gaia says “measures the disagreement, expressed as an angle, between the observations of a source and the best-fitting standard astrometric model”. The parameter D is “a dimensionless measure of the significance of the calculated astrometric_excess_noise (ϵ_i). A value $D \gtrsim 2$ indicates that the given (ϵ_i) is probably significant.” The parameter ‘RUWE’ is the ‘renormalised unit weight error’, and if large enough is sometimes taken as an indication that the source being observed consists of multiple stars. Finally, the last column gives the astrometric_matched_transits, i.e., the number of astrometric visits to the target.

From a perusal of Table B1, first we see that no value of RUWE substantially exceeds unity, indicating that the Gaia astrometric solution shows no real indication of stellar multiplicity. Second, for the three sources which show elevated values of D , indicating a somewhat significant value of the astrometric_excess_noise parameter, the Gaia distance and our distance differ by only 3%-9% out of ~ 2 kpc. Finally, we see that the expected uncertainties introduced by the light centroid motions within the triple are typically factors of a few smaller than the cited astrometric_excess_noise and just comparable with the cited parallax error. Therefore, we conclude that the motions of the center of light within the triple systems are just marginally at the level of affecting the distance measurements. However, all the evidence (see Table B1) suggests that the Gaia distances are not substantially affected by internal light centroid motions for our set of six sources.

The bottom line is that we generate our own independent distance measurements found as part of our photodynamical solutions. These are generally in fine agreement with those of Gaia, however, our claimed photometric distance uncertainties are smaller than those that Gaia reports, with no reason not to believe our photodynamic results.

Interestingly, a perusal of the column in Table B1 giving the rms motions of the center of light in these systems shows that they are all in the range of 47-130 μas . These are eminently detectable as ‘orbits’ with Gaia in their future analyses.

¹⁰ In this regard, for example, we note that the outer period of TIC 54060695 (60.8 days) is very close to 1/6 of a year.

Table B1. Details of the Distance Determinations

Target	Distance This work (pc)	Distance Gaia (pc)	π error ^a μas	a(col) ^b μas	rms(col) ^c μas	error(col) ^d μas	ϵ_i ^e μas	D ^f ...	RUWE ^g ...	matched transits
37743815	1789 ± 78	1857 ± 39	11	119	104	15	35	1.20	1.09	54
42565581	3150 ± 150	3281 ± 160	15	63	47	11	39	1.04	1.17	24
54060695	2427 ± 34	2221 ± 50	10	80	57	7	37	2.26	0.94	67
178010808	1415 ± 22	1464 ± 30	13	90	73	10	56	5.14	1.04	59
242132789	2667 ± 28	3258 ± 165	16	73	52	9	32	0.82	1.10	37
456194776	1690 ± 24	1590 ± 40	16	159	130	20	52	4.46	0.95	49

Notes. (a) Gaia uncertainty in the parallax (parallax_error). (b) Semimajor axis of the triple's center of light ('col') expressed in micro-arc seconds. (c) RMS fluctuations due to the triple's center of light motion. (d) Error contribution due to the triple's center of light motion (see text). (e) Gaia's astrometric_excess_noise. (f) Gaia's astrometric_excess_noise_significance. (g) Gaia's renormalized unit weight error – RUWE parameter. (h) The number of astrometric_matched_transits.

Table C1. Eclipse Times of TIC 37743815

BJD −2 400 000	Cycle no.	std. dev. (d)	BJD −2 400 000	Cycle no.	std. dev. (d)	BJD −2 400 000	Cycle no.	std. dev. (d)
58469.100180	0.0	0.017417	58485.427452	18.0	0.000927	59211.083151	818.0	0.000716
58470.005584	1.0	0.000922	58486.334080	19.0	0.001151	59211.992122	819.0	0.001195
58470.912387	2.0	0.001245	58487.244723	20.0	0.000905	59212.899021	820.0	0.001022
58471.820704	3.0	0.001031	58488.148083	21.0	0.001237	59213.807149	821.0	0.000824
58472.726629	4.0	0.001354	58489.057499	22.0	0.000869	59215.619239	823.0	0.000679
58473.638417	5.0	0.000964	58489.966834	23.0	0.001234	59216.525955	824.0	0.000809
58474.542843	6.0	0.001260	59202.013203	808.0	0.000802	59217.431905	825.0	0.000796
58475.448678	7.0	0.001309	59202.920768	809.0	0.000646	59218.340348	826.0	0.000910
58476.354330	8.0	0.001386	59203.829011	810.0	0.000844	59219.247375	827.0	0.000768
58478.169364	10.0	0.001328	59204.732837	811.0	0.001225	59220.153927	828.0	0.000794
58479.078449	11.0	0.000895	59205.641488	812.0	0.000816	59221.062602	829.0	0.000676
58479.983054	12.0	0.001364	59206.549341	813.0	0.000804	59221.968963	830.0	0.000851
58480.891648	13.0	0.001021	59207.454035	814.0	0.001035	59222.874870	831.0	0.000979
58481.797696	14.0	0.004524	59208.362881	815.0	0.000830	59225.595290	834.0	0.000982
58482.706871	15.0	0.001242	59209.270764	816.0	0.000754	59226.503925	835.0	0.000819
58483.612970	16.0	0.000995	59210.174682	817.0	0.000816	59227.409135	836.0	0.000712
58484.517480	17.0	0.000866						

Table C2. Eclipse Times of TIC 42565581

BJD −2 400 000	Cycle no.	std. dev. (d)	BJD −2 400 000	Cycle no.	std. dev. (d)	BJD −2 400 000	Cycle no.	std. dev. (d)
58469.003253	0.0	0.000269	58486.335932	9.5	0.000267	59210.992711	407.0	0.000191
58469.928359	0.5	0.000301	58487.234362	10.0	0.000299	59211.917368	407.5	0.000215
58470.826273	1.0	0.000275	58488.157862	10.5	0.000259	59212.816157	408.0	0.000232
58471.751681	1.5	0.000243	58489.057065	11.0	0.000337	59213.739667	408.5	0.000181
58472.649068	2.0	0.000331	58489.981803	11.5	0.000265	59215.566622	409.5	0.000189
58473.573118	2.5	0.000234	59201.881711	402.0	0.000191	59216.464242	410.0	0.000222
58474.472161	3.0	0.000277	59202.802591	402.5	0.000198	59217.386432	410.5	0.000176
58475.397381	3.5	0.000351	59203.701040	403.0	0.000133	59221.932759	413.0	0.000217
58476.294304	4.0	0.000251	59204.626061	403.5	0.000239	59222.856814	413.5	0.000190
58480.866051	6.5	0.000254	59205.525446	404.0	0.000151	59223.755438	414.0	0.000186
58481.765341	7.0	0.000410	59206.447958	404.5	0.000160	59224.678757	414.5	0.000226
58482.688807	7.5	0.000354	59207.347944	405.0	0.000198	59225.577908	415.0	0.000209
58483.587189	8.0	0.000355	59208.271297	405.5	0.000221	59226.501008	415.5	0.000219
58484.512607	8.5	0.000290	59209.169805	406.0	0.000183	59227.402701	416.0	0.000182
58485.410669	9.0	0.000522	59210.094530	406.5	0.000197			

APPENDIX C: TABLES OF DETERMINED ECLIPSE TIMES FOR ALL SIX SYSTEMS

In this appendix, we tabulate the individual mid-minima times of the primary and secondary eclipses for the inner EBs of the triples considered in this study (Tables C1-C6).

Table C3. Eclipse Times of TIC 54060695

BJD −2 400 000	Cycle no.	std. dev. (d)	BJD −2 400 000	Cycle no.	std. dev. (d)	BJD −2 400 000	Cycle no.	std. dev. (d)
58468.605940	-17.0	0.001095	58494.058064	7.0	0.003842	59205.647534	678.0	0.000588
58469.140378	-16.5	0.005653	58494.590093	7.5	0.003129	59206.179379	678.5	0.002318
58469.667026	-16.0	0.001367	58495.119416	8.0	0.000982	59206.706210	679.0	0.000586
58470.197503	-15.5	0.002369	58495.648973	8.5	0.004338	59207.238507	679.5	0.001438
58470.725605	-15.0	0.001084	58496.180311	9.0	0.001085	59207.767913	680.0	0.000569
58471.258699	-14.5	0.002208	58496.715667	9.5	0.003349	59208.297264	680.5	0.001070
58471.785257	-14.0	0.000656	58497.241219	10.0	0.001137	59208.828671	681.0	0.000674
58472.315201	-13.5	0.002350	58497.772757	10.5	0.006593	59209.358054	681.5	0.001747
58472.848220	-13.0	0.001029	58498.302567	11.0	0.001250	59209.888566	682.0	0.000546
58473.376212	-12.5	0.002832	58498.830635	11.5	0.004816	59210.419743	682.5	0.001637
58476.028160	-10.0	0.001878	58499.362499	12.0	0.001201	59210.950250	683.0	0.000525
58476.559043	-9.5	0.002884	58499.894586	12.5	0.009955	59211.477981	683.5	0.002378
58478.150295	-8.0	0.001785	58500.422492	13.0	0.001560	59212.009490	684.0	0.000576
58478.682432	-7.5	0.003870	58500.955348	13.5	0.004115	59212.540121	684.5	0.001944
58479.208497	-7.0	0.000615	58501.484125	14.0	0.000766	59213.070938	685.0	0.000548
58479.740703	-6.5	0.001954	58502.012980	14.5	0.004056	59213.600270	685.5	0.001494
58480.271792	-6.0	0.000750	58502.542231	15.0	0.001317	59215.721562	687.5	0.001951
58480.801877	-5.5	0.001508	58506.260908	18.5	0.003531	59216.252049	688.0	0.000451
58481.331202	-5.0	0.003872	58506.785416	19.0	0.000886	59216.784249	688.5	0.002169
58481.863746	-4.5	0.002555	58507.317745	19.5	0.003490	59217.312569	689.0	0.000477
58482.391152	-4.0	0.001007	58507.844674	20.0	0.001630	59217.841138	689.5	0.001451
58482.930523	-3.5	0.003879	58508.378102	20.5	0.002051	59218.373682	690.0	0.000477
58483.452838	-3.0	0.000904	58508.907052	21.0	0.000556	59218.907283	690.5	0.001287
58483.984392	-2.5	0.002246	58509.435525	21.5	0.001646	59219.434531	691.0	0.000540
58484.513781	-2.0	0.001109	58509.967497	22.0	0.000608	59219.964043	691.5	0.003971
58485.044984	-1.5	0.011035	58510.498675	22.5	0.001886	59220.496458	692.0	0.000494
58485.574971	-1.0	0.000736	58511.028526	23.0	0.015366	59221.027540	692.5	0.001712
58486.107091	-0.5	0.003441	58511.557418	23.5	0.002134	59221.555636	693.0	0.000521
58486.634619	0.0	0.000975	58512.087572	24.0	0.000831	59222.086269	693.5	0.001093
58487.167866	0.5	0.003574	58512.616997	24.5	0.003283	59222.615951	694.0	0.000443
58487.697342	1.0	0.001174	58513.148992	25.0	0.001401	59223.146045	694.5	0.003357
58488.231303	1.5	0.003585	58513.677824	25.5	0.005850	59223.676496	695.0	0.000562
58488.757146	2.0	0.000743	58514.209063	26.0	0.001968	59224.206998	695.5	0.002341
58489.282782	2.5	0.002575	58514.741532	26.5	0.002921	59224.737511	696.0	0.000539
58489.817359	3.0	0.000658	58515.268752	27.0	0.001399	59225.270801	696.5	0.001181
58491.937855	5.0	0.001191	58515.801427	27.5	0.005208	59225.798902	697.0	0.000578
58492.471299	5.5	0.001919	59204.060043	676.5	0.002236	59226.326089	697.5	0.001719
58492.998429	6.0	0.001038	59204.584860	677.0	0.000512	59226.857789	698.0	0.000477
58493.528706	6.5	0.006569	59205.118376	677.5	0.001569	59227.389174	698.5	0.001343

Table C4. Eclipse Times of TIC 178010808

BJD −2 400 000	Cycle no.	std. dev. (d)	BJD −2 400 000	Cycle no.	std. dev. (d)	BJD −2 400 000	Cycle no.	std. dev. (d)
58492.073256	0.0	0.000530	58508.999380	20.5	0.000173	59237.301079	902.5	0.000122
58492.486382	0.5	0.000444	58509.412402	21.0	0.000182	59237.713594	903.0	0.000113
58492.898591	1.0	0.000428	58509.825647	21.5	0.000180	59238.126559	903.5	0.000106
58493.312092	1.5	0.000442	58510.238029	22.0	0.000250	59238.539138	904.0	0.000120
58493.724843	2.0	0.000418	58510.650991	22.5	0.000185	59238.952447	904.5	0.000108
58494.138138	2.5	0.000468	58511.063326	23.0	0.000173	59239.365005	905.0	0.000105
58494.550590	3.0	0.000438	58511.476705	23.5	0.000185	59239.778311	905.5	0.000138
58494.963278	3.5	0.000427	58511.889525	24.0	0.000203	59240.190499	906.0	0.000115
58495.376087	4.0	0.000418	58512.303034	24.5	0.000284	59240.604009	906.5	0.000136
58495.788552	4.5	0.000385	58513.128904	25.5	0.000591	59242.253736	908.5	0.000663
58496.201972	5.0	0.000364	58513.540884	26.0	0.000258	59242.667866	909.0	0.000208
58496.614783	5.5	0.000375	58513.953829	26.5	0.000315	59243.081154	909.5	0.000205
58497.027188	6.0	0.000319	58514.367120	27.0	0.000291	59243.493740	910.0	0.000206
58497.440269	6.5	0.000421	58514.780110	27.5	0.000308	59244.319388	911.0	0.000138
58497.852818	7.0	0.000286	58515.192856	28.0	0.000288	59244.732030	911.5	0.000150
58498.266191	7.5	0.000291	58515.605843	28.5	0.000348	59245.145086	912.0	0.000124
58498.679015	8.0	0.000260	58516.018403	29.0	0.000479	59245.557762	912.5	0.000124
58499.091466	8.5	0.000334	59229.043614	892.5	0.000326	59245.970826	913.0	0.000122
58499.503950	9.0	0.000337	59229.456515	893.0	0.000185	59246.383649	913.5	0.000158
58499.917184	9.5	0.000470	59229.869065	893.5	0.000198	59246.796734	914.0	0.000132
58500.329864	10.0	0.000232	59230.282389	894.0	0.000156	59247.209664	914.5	0.000173
58500.742488	10.5	0.000299	59230.695285	894.5	0.000179	59247.622092	915.0	0.000159
58501.155265	11.0	0.000342	59231.108066	895.0	0.000177	59248.034725	915.5	0.000214
58501.568457	11.5	0.000229	59231.520912	895.5	0.000178	59248.447843	916.0	0.000164
58501.981398	12.0	0.000379	59231.933777	896.0	0.000164	59248.860334	916.5	0.000177
58502.394085	12.5	0.000288	59232.346900	896.5	0.000162	59249.273465	917.0	0.000205
58502.806852	13.0	0.000206	59232.759717	897.0	0.000152	59249.686580	917.5	0.000229
58504.870813	15.5	0.000309	59233.172386	897.5	0.000157	59250.099235	918.0	0.000185
58505.283323	16.0	0.000199	59233.584727	898.0	0.000136	59250.512084	918.5	0.000209
58505.696737	16.5	0.000183	59233.998317	898.5	0.000140	59250.924619	919.0	0.000227
58506.109155	17.0	0.000115	59234.410873	899.0	0.000138	59251.337762	919.5	0.000200
58506.522169	17.5	0.000172	59234.823729	899.5	0.000178	59251.750491	920.0	0.000208
58506.934614	18.0	0.000119	59235.236549	900.0	0.000127	59252.163121	920.5	0.000234
58507.347889	18.5	0.000220	59235.649505	900.5	0.000143	59252.576219	921.0	0.000220
58507.760879	19.0	0.000144	59236.062234	901.0	0.000122	59252.988873	921.5	0.000261
58508.173585	19.5	0.000181	59236.475241	901.5	0.000138	59253.401911	922.0	0.000244
58508.586585	20.0	0.000282	59236.888391	902.0	0.000115	59253.814624	922.5	0.000293

Table C5. Eclipse Times of TIC 242132789

BJD −2 400 000	Cycle no.	std. dev. (d)	BJD −2 400 000	Cycle no.	std. dev. (d)	BJD −2 400 000	Cycle no.	std. dev. (d)
58470.130373	-143.5	0.001382	58488.030554	-140.0	0.001011	59219.419094	3.0	0.000797
58472.684648	-143.0	0.000789	59204.057046	0.0	0.000937	59221.968075	3.5	0.001003
58475.235600	-142.5	0.001309	59206.617194	0.5	0.000948	59224.520611	4.0	0.000908
58480.343817	-141.5	0.000752	59209.178049	1.0	0.001010	59227.074177	4.5	0.001134
58482.906986	-141.0	0.000809	59216.861384	2.5	0.001011			

Table C6. Eclipse Times of TIC 456194776

BJD −2 400 000	Cycle no.	std. dev. (d)	BJD −2 400 000	Cycle no.	std. dev. (d)	BJD −2 400 000	Cycle no.	std. dev. (d)
58790.694887	-0.5	0.007130	58803.585185	7.0	0.000549	58813.901513	13.0	0.000773
58791.550543	0.0	0.002673	58804.448028	7.5	0.000535	58814.766254	13.5	0.009046
58792.414562	0.5	0.002784	58805.303613	8.0	0.000447	59098.452190	178.5	0.000268
58793.270358	1.0	0.001071	58806.166199	8.5	0.000500	59104.469630	182.0	0.000269
58794.133511	1.5	0.001933	58807.024167	9.0	0.000422	59116.511643	189.0	0.000049
58794.987072	2.0	0.002167	58807.888026	9.5	0.001142	59159.493484	214.0	0.000048
58795.852371	2.5	0.001374	58808.742542	10.0	0.000294	59168.946719	219.5	0.000157
58796.708543	3.0	0.001245	58810.463083	11.0	0.000740	59276.410632	282.0	0.000140
58797.570872	3.5	0.001705	58811.324887	11.5	0.001979	59515.405227	421.0	0.000097
58798.426856	4.0	0.000800	58812.181601	12.0	0.000487	59527.433741	428.0	0.000100
58799.290589	4.5	0.001175	58813.045175	12.5	0.001882	59539.466978	435.0	0.000116
58800.146908	5.0	0.000683						

Notes. Eclipses between cycle numbers −0.5 and 13.5 was observed with *TESS*, while the last 9 events were observed in the frame of our ground-based follow up campaign.